NASA Contractor Report 190783

Integrated Analysis and Design of Thick Composite Structures for Optimal Passive Damping Characteristics

D.A. Saravanos
Ohio Aerospace Institute
Brook Park, Ohio

March 1993

Prepared for
Lewis Research Center
Under Cooperative Agreement NCC3–208/4

National Aeronautics and
Space Administration

TABLE OF CONTENTS

INTEGRATED ANALYSIS AND DESIGN OF THICK COMPOSITE STRUCTURES FOR OPTIMAL PASSIVE DAMPING CHARACTERISTICS

D.A. Saravanos
Ohio Aerospace Institute
Brook Park, Ohio 44142

ABSTRACT

The development of novel composite mechanics for the analysis of damping in composite laminates and structures, and the more significant results of this effort are summarized.

Laminate mechanics based on piecewise continuous in-plane displacement fields are described that can represent both intralaminar stresses and interlaminar shear stresses and the associated effects on the stiffness and damping characteristics of a composite laminate. Among other features, the mechanics can accurately model the static and damped dynamic response of either thin or *thick* composite laminates, as well as, specialty laminates with embedded compliant damping layers.

The discrete laminate damping theory is further incorporated into structural analysis methods. In this context, an exact semi-analytical method for the simulation of the damped dynamic response of composite plates was developed. A finite element based method and a specialty four-node plate element was also developed for the analysis of composite structures of variable shape and boundary conditions. Numerous evaluations and applications demonstrate the quality and superiority of the mechanics in predicting the damped dynamic characteristics of composite structures.

Finally, additional development was focused towards the development of optimal tailoring methods for the design of thick composite structures based on the developed analytical capability. Applications on composite plates illustrated the influence of composite mechanics in the optimal design of composites and the potential for significant deviations in the resultant designs when more simplified (classical) laminate theories are used.

LIST OF FIGURES

1. SUMMARY OF ORIGINALLY PROPOSED RESEARCH

The originally proposed research plan addressed the need to develop novel damping mechanics for the accurate analysis and design of thick composite structures. The proposed plan emphasized the need of damping mechanics applicable not only on thin composite structures, but also on composite structures of significant thickness; structures with embedded compliant interlaminar layers; and structures at elevated temperatures.

In order to realize the full benefits of damping in the analysis and design of advanced composite structures, the following technical objectives were defined:

(1) Development of admissible integrated damping mechanics for the accurate simulation of damping in thick composite laminates and/or laminates with interlaminar damping layers.

(2) Development of novel mixed structural mechanics enabling the accurate computational simulation of damping in thick composite structures, at room or elevated temperature conditions.

(3) Development of novel tailoring methods for the design of thick composite structures. The methods were proposed to integrate the damping mechanics with suitable optimization methodologies, and address current structural requirements via multiple design criteria.

2. SUMMARY OF SIGNIFICANT ACCOMPLISHMENTS

2.1. Research and Technology Developments

The three proposed milestones of the proposed research plan were accomplished as follows:

(1) **Thick-Laminate Damping Mechanics:** The critical issue of accurate representation of displacement and stress variations through the composite plies was addressed by developing rigorous discrete laminate damping mechanics incorporating piecewise continuous displacement fields (refer to Section 3; Fig. 3.1). The effects of temperature and moisture were incorporated. The mechanics were evaluated on thick laminates, laminates with interleave layers, and laminates at higher temperatures (for more details refer to Sections 4 and 5; Figs. 4.1, 4.2, 5.3-5.6). In addition to superior damping predictions, more accurate evaluations of laminate displacements and strains were obtained, which

significantly enhanced the in-house modelling capacity for thick laminates (see also, code ICAN/DLDT, Section 2.3).

(2) **Computational Simulation of Structural Damping:** The developed thick-laminate damping theory was integrated into a finite element discretization scheme. A specialty plate finite element was developed, enabling the synthesis of damping, stiffness, and mass matrices (refer to Section 3).

The element formulation allows application in two different ways, specifically: (1) as a generalized plate element with 4 nodes at the middle surface of the composite; and (2) as a generalized "thick-shell" type element with nodes at the upper, lower, and optionally middle surfaces of the laminate. Evaluations of this novel finite element, has shown great advantages in the simulation of coupled thermomechanical response, not only in thick composite structures (refer to Section 4; Figs. 4.1, 4.4-4.8), but also, in composites with compliant interply layers (refer to Section 6; Figs 6.1-6.8) and thin composite structures with significant interlaminar inhomogeneity (see Fig. 4.2). The element is presently integrated in the STAT (Structural Tailoring of Advanced Turboprops) in-house code.

(3) **Optimal Design of Thick Composite Structures:** A design method for the tailoring of composite components of general thickness, lamination, geometry and loading/boundary conditions was developed. The method is integrated in the STAT (Structural Tailoring of Advanced Turboprops) in-house code (code STAT/DLDT, Sec. 2.3). In this manner, the tailoring capability of the code is extended to cover the area of thick composite structures. The design methodology is consistent with previous developments addressing current challenging structural requirements expressed as multiple design criteria. A multi-objective formulation is available and candidate design variables may include parameters from the multiple structural scales of a composite structure.

An *additional* smaller scale method was also developed for tailoring thick composite plates. The method is encoded into a stand-alone code (code THICOPT, Section 2.3) which can provide quick, inexpensive optimal designs for simply-supported composite plates. Applications and comparisons with similar design methods based on thin composite mechanics demonstrated significant advantages of the new method (refer to Section 7; also see Fig. 7.1).

In both cases mentioned above, the optimization is numerically performed with direct non-linear programming algorithms, that is, algorithms performing a direct search in the design domain based on first order sensitivity.

2.2. Summary of Benefits and Results

The following significant results were attained:

(1) Development of functional in-house software. Specifically the following codes were developed:

ICAN/DLDT: An integrated code for the dynamic analysis of thick composite laminates and plates incorporating the developed discrete laminate damping theory (DLDT). An addendum to ICAN's Usser'r Manual is under preparation

STAT/DLDT: A structural analysis/tailoring code for composite propulsion components. The code now includes the developed finite element as previously described

THICOPT: (Thick Composite Plate Tailoring). A versatile, computationally inexpensive code for optimal design applications in thick composite plates.

(2) Evaluation and demonstration of the quality of the developed novel damping mechanics on select thick composite structures. The significant advantages of the developed laminate and structural damping mechanics were quantified for composites structures of: (i) higher thickness; (ii) alternating angle-ply laminates; and (iii) laminates with compliant interlaminar layers.

(3) Initial evaluations of the developed optimal design methodology on typical composite plates were performed. The results demonstrated significant benefits in the design of composite structures.

(4) Numerous technical publications (see subsection 2.4) describing the developed methodologies, and enumerating evaluations, experimental correlations and conclusions of technical significance.

2.3. Resultant Publications

Saravanos, D. A. and Pereira J. M., "Effects of Interply Damping Layers on the Dynamic response of Composite Plates," AIAA Journal, in press, Nov. 1992.

Saravanos, D. A., "Simulation of Passive Damping in Thick Composite Structures," AIAA J., to appear.

Saravanos, D. A., "Damped Dynamic Characteristics of Thick Composite Laminates and Plates," ASME Journal of Applied Mechanics, to appear.

Saravanos, D. A. and Chamis C. C., "Damped Dynamic Characteristics of Specialty Composite Materials and Structures," Proceedings, Symposium on Vibroacoustic Characterization of Materials and Structures, ASME Winter Annual Meeting, Anaheim, California, Nov. 8-13, 1992

Saravanos, D. A. "Analysis and Optimal Design of Thick Composite Structures with Passive Damping Considerations," Proceedings, 4th AIAA/AIR FORCE/NASA/OAI Symposium on Multidisciplinary Analysis and Optimization, Sept. 21-23, 1992, Cleveland, Ohio.

3. THEORETICAL BACKGROUND

3.1. Introduction

The significance of passive damping in improving the dynamic performance of flexible structures requiring tight vibration control, high fatigue endurance, and accurate positioning of devices and sensors has been recently emphasized. In addition, low levels of damping are also considered beneficial in actively controlled structures, as they typically improve the robustness of the controller. As a result, the prediction and tailoring of the passive damping capacity of polymer matrix composite structures is receiving current attention.

Various damping mechanics theories for unidirectional composites, laminates and structures have been reported and a representative selection is mentioned here[1-11]. However, most of the previously mentioned work is limited to the classical laminate theory assumptions which neglect interlaminar shear effects, hence, this work is suitable only for thin laminates. Moreover, interlaminar shear effects are more critical in laminated composite structures because of their through-the-thickness inhomogeneity and anisotropy, than in homogeneous isotropic materials. Therefore, interlaminar shear damping is expected to be significant in composites, particularly in laminates of thicker sections. Yet, limited research has been reported in this direction[12].

This paper presents recent developments on discrete damping mechanics enabling more accurate prediction of damping properties in thick composite structures. The modelling of damping at the laminate level is based on a novel discrete-layer laminate damping theory (DLDT) which assumes a discrete, yet, piecewise continuous displacement field through the laminate. The DLDT effectively captures both interply and intraply stresses. The overall damping capacity of the laminate includes contributions from extension, flexure-shear, and various material coupling from possible asymmetries that may exist due to the heterogeneous nature of the composite laminate.

Semi-analytical methods were first developed for the prediction of modal damping and other dynamic characteristics of thick specialty composite plates[13]. This method was exact and computationally inexpensive, but its applications were limited. In order to simulate damping in composite structures of general thickness, shape, lamination, and boundary conditions, generalized structural mechanics based on finite element discretization were developed. This approach is described in the following sections. A specialty 4-node element incorporating the aforementioned discrete-layer laminate damping theory is described. Generalized damping, stiffness and mass element matrices are formulated.

Therefore, in addition to improved modal damping predictions, more accurate calculations of the dynamic response and stresses may be also obtained.

Evaluations of the damping mechanics are presented. The validations include either direct comparisons with known exact solutions for composite plates, or comparisons between the DLDT and classical damping theory. The significance of interlaminar shear damping contributions is also quantified. Finally, the effects of thickness and lamination on the damped dynamic characteristics of composite plates and beams are investigated.

3.2. Composite Mechanics

This section briefly reviews the synthesis of damping for on-axis composites (damping along the material axes), off-axis composites (unidirectional composites loaded at an angle), and composite laminates of general stacking sequence. The measures of damping used in this paper will be primarily the loss factor η, and secondarily the specific damping capacity (SDC) ψ ($\eta = \psi/2\pi$).

Unidirectional Composites

For a unidirectional composite loaded along the material axes (see Fig. 3.1a), closed-form expressions have been developed for the synthesis of elastic and dissipative properties[7]. In summary, five independent elastic parameters completely characterize the stiffness of a unidirectional composite (orthotropic but transversely isotropic material). An additional four independent damping loss factors characterize the composite damping, that is, longitudinal loss factor η_{l11} (direction 11), transverse in-plane damping η_{l22} (direction 22), transverse through-the-thickness damping $\eta_{l33}=\eta_{l22}$ (direction 33), in-plane shear damping η_{l66} (direction 12), interlaminar shear damping η_{l44} (direction 23), and interlaminar shear damping $\eta_{l55}= \eta_{l66}$ (direction 13). Both damping and elastic properties are explicitly related to the fiber and matrix properties, and to the fiber volume ratio (FVR).

For the case of off-axis composites, ie. composites loaded at an angle θ, a 6 by 6 damping matrix $[\eta_c]$ best describes the damping of the composite. More details about this off-axis damping matrix are provided in the Appendix II and refs. 7,13. Off-axis loading affects the overall damping capacity of the composite in two distinct ways that are uncommon to isotropic materials: by altering the dissipative capability of the ply directly associated to normal and shear strains; and by inducing damping coupling between normal and shear strains.

Thick Laminates

To model the damping of thick composite laminates, a discrete layer laminate damping theory (DLDT) incorporating a piecewise continuous displacement field through-the-thickness is developed. The kinematic assumptions for the laminate theory are schematically shown in Fig 3.1b. Discrete layer or generalized laminate theories have been proposed (see refs. 14, 15) for the more accurate calculation of stresses in thick laminates. However, with additional developments presented herein, the DLDT combines the potential for accurate damping predictions in composite laminates while maintaining generality and elegance. The assumed displacement field has the form,

$$\begin{aligned} u(x,y,z,t) &= u^{o}(x,y,t) + \bar{u}(x,y,z,t) \\ v(x,y,z,t) &= v^{o}(x,y,t) + \bar{v}(x,y,z,t) \\ w(x,y,z,t) &= w^{o}(x,y,t) \end{aligned} \tag{1}$$

where superscript o represents the uniform through-the-thickness midplane displacement, and the bar indicates the through-the-thickness variation in the displacement field. Assuming that the displacements are separable functions of z, the previous equations take the form [15]:

$$\begin{aligned} u(x,y,z,t) &= u^{o}(x,y,t) + \sum_{j=1}^{N} u^{j}(x,y,t)F^{j}(z) \\ v(x,y,z,t) &= v^{o}(x,y,t) + \sum_{j=1}^{N} v^{j}(x,y,t)F^{j}(z) \\ w(x,y,z,t) &= w^{o}(x,y,t) \end{aligned} \tag{2}$$

where, u^j and v^j are displacements, along the x and y directions respectively, at the interfaces between composite plies or sublaminates (group of plies). $F^j(z)$ are interpolation functions. In this manner, the assumed in-plane displacement field is general, in that it may represent extensional, flexural, shear, and coupled deformations as well as interlaminar shear strains through the thickness of the laminate.

The engineering strains $\{\epsilon_c\}$ in each composite ply are directly derived from eqs. (2) The normal strain ϵ_{c3} is zero as a result of the assumed constant through-the-thickness deflection w. The midplane strains are given by,
and the generalized strains are,
The comma in the subscripts indicates differentiation.

$$\epsilon_{ci} = \epsilon_{ci}^{o} + \sum_{j=1}^{N} \epsilon_{ci}^{j} F^{j}(z) \qquad i=1,2,6$$
$$\epsilon_{ci} = \epsilon_{ci}^{o} + \sum_{j=1}^{N} \epsilon_{ci}^{j} F_{,z}^{j}(z) \qquad i=4,5 \tag{3}$$
$$\epsilon_{c3} = 0$$

$$\epsilon_{c1}^{o} = u_{,x}^{o} \qquad \epsilon_{c2}^{o} = v_{,y}^{o} \qquad \epsilon_{c6}^{o} = u_{,y}^{o} + v_{,x}^{o}$$
$$\epsilon_{c4}^{o} = w_{,y}^{o} \qquad \epsilon_{c5}^{o} = w_{,x}^{o} \tag{4}$$

$$\epsilon_{c1}^{j} = u_{,x}^{j} \qquad \epsilon_{c2}^{j} = v_{,y}^{j} \qquad \epsilon_{c6}^{j} = u_{,y}^{j} + v_{,x}^{j}$$
$$\epsilon_{c4}^{j} = v^{j} \qquad \epsilon_{c5}^{j} = u^{j} \tag{5}$$

The dissipated strain energy per unit area of the laminate ΔS_L is,

$$\Delta S_L = 1/2 \int_{-h/2}^{h/2} 2\pi \ \epsilon_c^{T} [Q_c][\eta_c] \epsilon_c dz \tag{6}$$

where $[Q_c]$ is the off-axis composite stiffness matrix. Combination of eqs. (6, 2-5) ultimately provides the dissipated strain energy per unit area,

$$\Delta S_L = \frac{1}{2} 2\pi \left(\epsilon_c^{oT} [A_d] \epsilon_c^{o} + 2\epsilon_c^{oT} \sum_{j=1}^{N} [B_d^{j}] \epsilon_c^{j} + \sum_{j=1}^{N} \sum_{m=1}^{N} \epsilon_c^{jT} [D_d^{jm}] \epsilon_c^{m} \right) \tag{7}$$

where $[A_d]$ is the extensional laminate damping matrix, which includes out-of-plane shear terms. The generalized coupling damping matrices $[B_d^{j}]$ and flexural/shear matrices $[D_d^{jm}]$ are new. The matrix expressions in eq. (7) are given by
Similarly, the maximum laminate strain energy per unit area S_L is by definition,

$$S_L = 1/2 \int_{-h/2}^{h/2} \epsilon_c^{T} [Q_c] \epsilon_c dz \tag{9}$$

Combination of eqs. (3-5, 9) provides the maximum strain energy as a separable form of material properties and strains,
where, [A] is the extensional laminate stiffness matrix with additional out-of-plane shear

$$
\begin{aligned}
[A_d] &= \sum_{k=1}^{N_l} \int_{h_{k-1}}^{h_k} [Q_c]_k [\eta_c]_k dz \\
(B_d^j)_{in} &= \sum_{k=1}^{N_l} \int_{h_{k-1}}^{h_k} ([Q_c]_k [\eta_c]_k)_{in} F^j(z) dz \qquad i,n=1,2,6 \\
(B_d^j)_{in} &= \sum_{k=1}^{N_l} \int_{h_{k-1}}^{h_k} ([Q_c]_k [\eta_c]_k)_{in} F_{,z}^j(z) dz \qquad i,n=4,5 \\
(D_d^{jm})_{in} &= \sum_{k=1}^{N_l} \int_{h_{k-1}}^{h_k} ([Q_c]_k [\eta_c]_k)_{in} F^j(z) F^m(z) dz \qquad i,n=1,2,6 \\
(D_d^{jm})_{in} &= \sum_{k=1}^{N_l} \int_{h_{k-1}}^{h_k} ([Q_c]_k [\eta_c]_k)_{in} F_{,z}^j(z) F_{,z}^m(z) dz \qquad i,n=4,5
\end{aligned}
\tag{8}
$$

$$
S_L = 1/2(\epsilon_c^{oT}[A]\epsilon_c^o + 2\epsilon_c^{oT}\sum_{j=1}^{N}[B^j]\epsilon_c^j + \sum_{j=1}^{N}\sum_{m=1}^{N}\epsilon_c^{jT}[D^{jm}]\epsilon_c^m) \tag{10}
$$

terms, $[B^j]$ are the generalized coupling stiffness matrices, and $[D^{jm}]$ the flexural/shear matrices[15]. These matrix expressions are given by:

$$
\begin{aligned}
[A] &= \sum_{k=1}^{N_l} \int_{h_{k-1}}^{h_k} [Q_c]_k dz \\
(B^j)_{in} &= \sum_{k=1}^{N_l} \int_{h_{k-1}}^{h_k} ([Q_c]_k)_{in} F^j(z) dz \qquad i,n=1,2,6 \\
(B^j)_{in} &= \sum_{k=1}^{N_l} \int_{h_{k-1}}^{h_k} ([Q_c]_k)_{in} F_{,z}^j(z) dz \qquad i,n=4,5 \\
(D^{jm})_{in} &= \sum_{k=1}^{N_l} \int_{h_{k-1}}^{h_k} ([Q_c]_k)_{in} F^j(z) F^m(z) dz \qquad i,n=1,2,6 \\
(D^{jm})_{in} &= \sum_{k=1}^{N_l} \int_{h_{k-1}}^{h_k} ([Q_c]_k)_{in} F_{,z}^j(z) F_{,z}^m(z) dz \qquad i,n=4,5
\end{aligned}
\tag{11}
$$

Considering eq. (2), the laminate kinetic energy per unit area takes the form:

$$
K_L = 1/2(\{\dot{u}^o\}^T[A_M]\{\dot{u}^o\} + 2\{\dot{u}^o\}^T\sum_{j=1}^{N}[B_M^j]\{\dot{u}^j\} + \sum_{j=1}^{N}\sum_{m=1}^{N}\{\dot{u}^j\}^T[D_M^{jm}]\{\dot{u}^m\}) \tag{12}
$$

where the generalized laminate mass and inertia matrices are defined as,

$$[A_M] = \sum_{k=1}^{N_l} \int_{h_{k-1}}^{h_k} diag(\rho_k) dz \qquad [B_M^j] = \sum_{k=1}^{N_l} \int_{h_{k-1}}^{h_k} diag(\rho_k) F^j(z) dz$$
$$[D_M^{jm}] = \sum_{k=1}^{N_l} \int_{h_{k-1}}^{h_k} diag(\rho_k) F^j(z) F^m(z) dz \tag{13}$$

The term diag(ρ_k) indicates a diagonal matrix, with all diagonal terms equal to the density of the k-th ply. The kinetic energy in eq. (12) includes contributions of rotational inertia. As seen, the proposed laminate damping mechanics are general and they can handle any laminate configuration in terms of composite plies, ply angles, laminate stacking sequence, and thickness.

3.3. Simply-Supported Composite Plates

Based on the previously described laminate mechanics, exact solutions of the damped dynamic characteristics for specialty composite plates have been obtained and summarized herein for the sake of completeness[13]. These exact and computationally inexpensive predictions of static and dynamic characteristics (modal damping, natural frequencies) provided valuable insight in the mechanics of the problem and establish a baseline for validating approximate numerical methods. Most other laminations, boundary conditions, and structural configurations require approximate discretized solutions, and such finite element based computational mechanics are described in the next section.

For a rectangular α by β simply supported (SS) composite plate with negligible coupling ($A_{16} = A_{26}=0$, $B^j_{16} = B^j_{26}=0$, $D^{jm}_{16} = D^{jm}_{26}=0$), the following Navier fundamental solutions form a complete set of mode shapes in the x-y plane:

$$\begin{aligned} u^o_{mn}(x,y,t) &= U^o_{mn}\cos(ax)\sin(by)e^{i\omega t} \\ v^o_{mn}(x,y,t) &= V^o_{mn}\sin(ax)\cos(by)e^{i\omega t} \\ w^o_{mn}(x,y,t) &= W^o_{mn}\sin(ax)\sin(by)e^{i\omega t} \\ u^j_{mn}(x,y,t) &= U^j_{mn}\cos(ax)\sin(by)e^{i\omega t} \\ v^j_{mn}(x,y,t) &= V^j_{mn}\sin(ax)\cos(by)e^{i\omega t} \end{aligned} \qquad \textbf{(14)}$$

Where, $a= m\pi/\alpha$, $b= n\pi/\beta$, and the fundamental solutions in eq. (14) are chosen because they satisfy the boundary conditions of the simply-supported plate.

Combination of eqs. (4,5,14) yields the modal mid-plane and generalized strains as separable functions of x, y coordinates, time, and amplitudes.

$$\{\epsilon^o\}_{mn}=[B^o_{mn}]\{U^o_{mn}\}e^{i\omega t} \qquad \{\epsilon^j\}_{mn}=[B^j_{mn}]\{U^j_{mn}\}e^{i\omega t} \qquad \textbf{(15)}$$

where, the terms in matrices $[B_{mn}]$ are sinusoidal functions of x, y coordinates and mode order. The amplitude displacement vectors are $\{\mathbf{U^o}\} = \{U^o, V^o, W^o\}^T$ and $\{\mathbf{U^j}\} = \{U^j, V^j\}^T$.

By substituting eqs. (15) into the strain and kinetic energy expressions for the laminate, eqs. (10) and (12) respectively, integrating over the plate area, and applying Lagrangian dynamics, the modal analysis (free vibration) solution of the plate takes the form:
where, the through-the-thickness modal displacements are $\{\mathbf{U_{mn}}\} = \{\mathbf{U^o_{mn}}; \mathbf{U^1_{mn}},...,\mathbf{U^N_{mn}}\}$

$$-\omega_{mn}^2[M_{mn}]U_{mn} + [K_{mn}]U_{mn} = 0 \tag{16}$$

and subscripts m, n indicate the mode order. Numerical solution of this eigenvalue problem provides the natural frequencies ω_{mn} and the through-the-thickness modes $\{U_{mn}\}$ for each order mn of plane modes, in the context of eqs. (14).

The modal damping associated with the mn-th vibration mode η_{mn} is:

$$\eta_{mn} = \frac{1}{2\pi}\frac{\int_A \Delta S_{Lmn} dA}{\int_A S_{Lmn} dA} \tag{17}$$

where ΔS_{Lmn} and S_{Lmn} are respectively the dissipated and maximum laminate strain energies, respectively of the associated mode.

3.4. Finite Element Method

Computational finite-element based mechanics for the damping analysis of thick composite structures of general laminations and shapes were developed, based on the DLDT and are summarized herein. In view of the generalized laminate strains and stresses described in the previous sections, the variational formulation of the equilibrium equations for the candidate structure takes the form:

$$-\int_A \{\delta\epsilon^{oT} N^o + \sum_{j=1}^{N} \delta\epsilon^{jT} N^j\} dA - \int_A \{\delta u^{oT} [A_m] \ddot{u}^o + 2\delta u^{oT} \sum_{i=1}^{N} [B_m^j] \ddot{u}^j + \sum_{j=1}^{N} \sum_{m=1}^{N} \delta u^{jT} [D_m^{jm}] \ddot{u}^m\} dA + \delta u_i^T F_i + \int_S \delta u_s^T F_s ds = 0 \tag{18}$$

For viscoelastic constituents, the constitutive viscoelastic law between generalized stresses and strains at the laminate level may be eventually expressed by the following convolute products,

$$\begin{aligned} N^o(t) &= [\tilde{A}(t)] * \epsilon^o(t) + \sum_{m=1}^{N} [\tilde{B}^m(t)] * \epsilon^m(t) \\ N^j(t) &= [\tilde{B}^j(t)] * \epsilon^o(t) + \sum_{m=1}^{N} [\tilde{D}^{jm}(t)] * \epsilon^m(t), \qquad j=1,...,N \end{aligned} \tag{19}$$

where * indicates a convolution operation, for example,

$$\sigma_c = [\tilde{Q}_c] * \epsilon_c = \int_{-\infty}^{t} [\tilde{Q}(t-\tau)] d\epsilon(\tau) \tag{20}$$

Hence, the first left-hand integral in eq. (18) represents both stored and dissipated strain energies during the virtual displacement. The elastic laminate relations will result from eq. (19) if time effects are neglected. Also, viscous damping is a special case of eqs. (18). In the frequency domain (harmonic vibration), eqs. (19) will result in equivalent expressions of complex laminate stiffness, with storage and loss stiffness matrices described in eqs. (8) and (11) respectively.

The variational relationship may be discretized to an approximate equivalent system of dynamic equations, if the reference and generalized displacements are discretized as follows:

where, subscript i indicates the i-th node, and ϕ_i are interpolating functions. The reference and generalized strain shape functions, $[R^o]_i$ and $[R]_i$ interpolating the strains to the nodal displacements, are obtained by differentiating eq. (21) in accordance with

$$\{u^o,v^o,w^o\}=\sum_{i=1}^{nodes}[\Phi_i]\{u_i^o,v_i^o,w_i^o\}$$
$$\{u^j,v^j\}=\sum_{i=1}^{nodes}[\Phi_i]\{u_i^j,v_i^j\},\qquad j=1,...,N \tag{21}$$

eqs. (4,5). Then the damping or loss element matrix $[C_{eij}]$ for nodes i and j takes the form:

$$[C_{eij}]=\int_{A_e}\begin{bmatrix} R_i^{oT}[A_d]R_j^o & R_i^{oT}[B_d^1]R_j & \dots & R_i^{oT}[B_d^N]R_j \\ R_i^T[B_d^1]R_j^o & R_i^T[D_d^{ij}]R_j & \dots & R_i^T[D_d^{1N}]R_j \\ \cdot & \cdot & \dots & \cdot \\ \cdot & \cdot & \dots & \cdot \\ R_i^T[B_d^N]R_i^o & R_i^T[D_d^{N1}]R_j^o & \dots & R_i^T[D_d^{NN}]R_j \end{bmatrix} dA_e \tag{22}$$

where A_e is the area of the element. The area integration is performed numerically. The stiffness and mass matrices of the element, $[K_{eij}]$ and $[M_{eij}]$ respectively, have analogous forms. Subsequently, the dissipated and maximum stored strain energies of the element are given by:

$$\Delta S_{eij}=1/2\ U_i^T[C_{eij}]U_j \quad , \qquad S_{eij}=1/2\ U_i^T[K_{eij}]U_j \tag{23}$$

and the modal damping of the n-th mode η_n is expressed as the ratio of the dissipated over the maximum modal strain energy of the structure.

$$\eta_n = \frac{1}{2\pi}\frac{\Sigma\ \Delta S_{eijn}}{\Sigma\ S_{eijn}} \tag{24}$$

In this context, a bilinear four-node plate element was developed. Selective integration was utilized to avoid overstiffening of the element in the case of low thickness. Such overstiffening was observed with full integration.

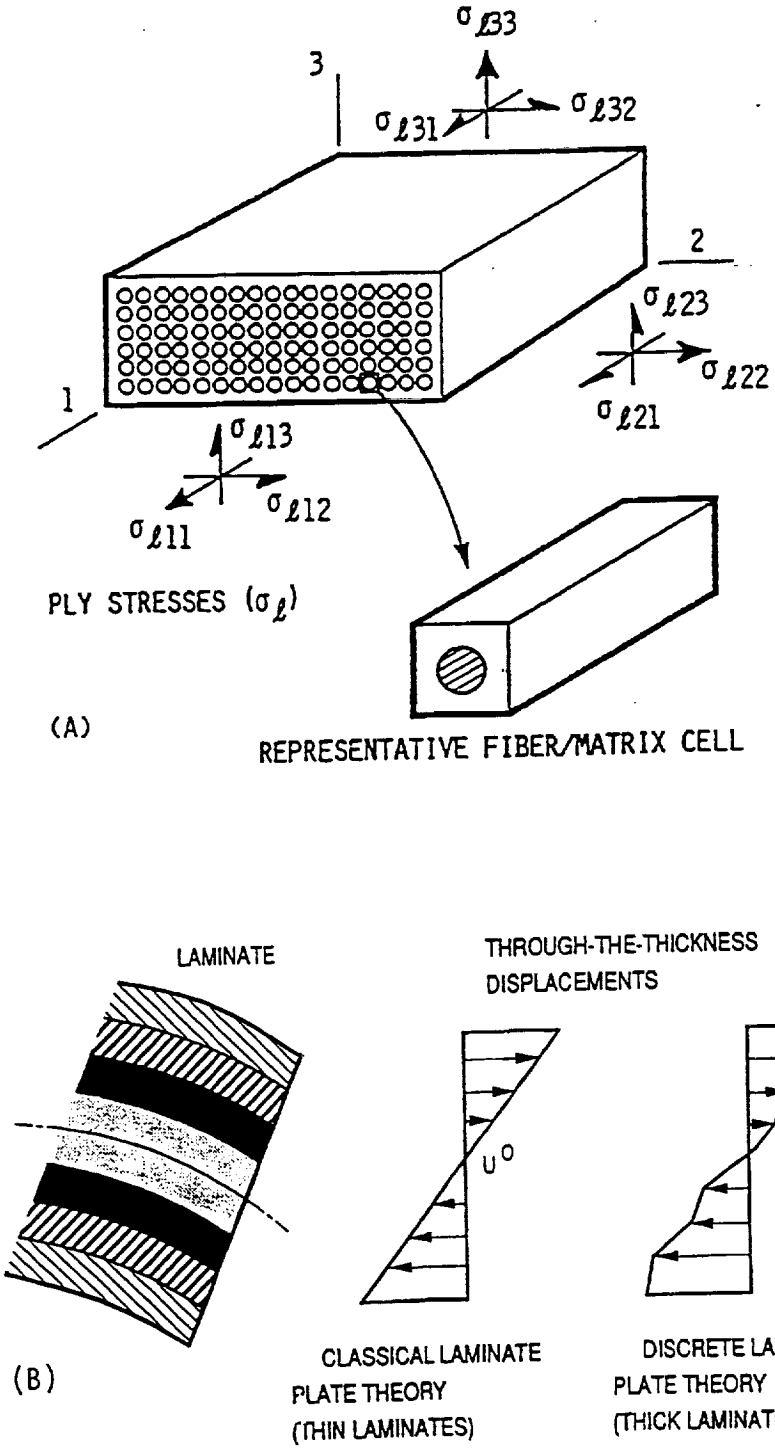

Fig. 3.1 (a) Unidirectional composite. (b) Kinematic assumptions of laminate damping theories; classical laminate damping theory (CLDT) and discrete layer damping theory (DLDT).

4. DAMPING PREDICTIONS IN THICK COMPOSITE STRUCTURES

To demonstrate the quality and versatility of the composite mechanics, applications on Gr/Epoxy composite plates and beams were performed. When applicable, numerical results obtained with the aforementioned element were compared with the exact solutions. In all other cases the predictions were compared with results obtained using a triangular plate element based on classical laminate damping theory (CLDT)[11]. Both elements will be referred to respectively as DLDT and CLDT finite elements thereafter. The composite material used in all applications was HM-S Graphite/Epoxy of 50% fiber volume ratio (FVR). Measured data for this composite are provided in Ref. 9. The properties of the the fibers and the matrix were backcalculated using micromechanics[9] to match the measured properties of the composite. Unless otherwise stated, the nominal thickness of each composite ply was taken as 0.254 mm (0.01 inches).

4.1. $[0_4/90_4]_s$ Simply-Supported Composite Plate

Fig. 4.1 shows predicted natural frequencies and modal damping values of the fundamental mode of a $[0_4/90_4]_s$ square composite SS plate as functions of thickness aspect ratio (α/h), where t is the plate thickness. The modal characteristics of the first 4 modes, that is, modes (1,1), (1,2), (2,1), and (2,2) are shown respectively. It is pointed out, that this laminate has different flexural damping and stiffness characteristics in x and y directions, thus, modes (1,2) and (2,1) have different natural frequencies and modal loss factors. The finite element model consisted of a uniform mesh of 8 by 8 element subdivisions. Clearly, there is excellent agreement between the exact DLDT solutions and the finite element model in the shown thickness regime. The exact CLDT solution is also shown, to illustrate the significant differences between the two theories in damping prediction at high thicknesses. The differences between DLDT and CLDT predictions provide the estimate of interlaminar shear damping. Finally, the results calculated using the DLDT finite element converge to the exact CLDT predictions as the plate thickness is decreased.

Fig. 4.2 shows the effect of temperature on the fundamental modal damping and natural frequency of $[0_4/90_4]_s$ and $[0/90]_{4s}$, 203 mm by 203 mm (8 in by 8 in) square plates. Predictions of the fundamental SDC and natural frequency of each plate, subjected to uniform through-the-thickness temperature variations are plotted as functions of temperature. Interestingly, the CLDT significantly underestimates the fundamental SDC at higher temperatures. The underestimation is slightly lower in the second plate. It is recalled, that in higher temperatures both the shear modulus of the 90-deg. plies decreases and the shear damping increases respectively. The temperature variation has

little effect on the natural frequency.

4.2 $[0/90/45/-45]_s$ Free-Free Composite Beam

Fig. 4.3 presents the modal damping and natural frequencies of the first and second bending modes of an unsupported (free-free) $[\theta/90+\theta/45+\theta/-45+\theta]_s$ thin beam (l/h=125). This laminate configuration was used previously in both experimental and analytical studies[8,9]. The CLDT model has failed to capture the portion of damping due to interlaminar shear stresses and relative rotation between adjacent plies. Hence, this case serves as a demonstration of the dependence of damping on the specific laminate lay-up only, and also as an example of the capacity of DLDT to capture both flexural and shear damping.

Equivalent element meshes consisting of 15 by 4 element subdivisions were used to predict the dynamic characteristics of the beam. The dimensions of the beam were approximately equal to specimens used by Ni and Adams[9], that is, 200 mm (8 in) long, 12 mm (0.5 in) wide, and 1.60 mm (0.064 in) thick. As seen in Fig. 4.3, the DLDT damping predictions are higher than the CLDT prediction and correlates very well with the reported measurements[9], hence, the new theory has succeeded in capturing the interlaminar shear damping contributions in the range of high interlaminar shear stresses and relative rotation between outer plies ($\theta \simeq 45°, 135°$). It is emphasized, that in this case the interlaminar shear damping is mostly the result of inhomogeneities in the material anisotropy between the plies of alternating fiber orientation; therefore, the case study serves as another example of the superiority of the method.

4.3. $[\theta_4/-\theta_4]_s$ Simply-Supported Composite Plate

The lower modal damping values and natural frequencies predicted for a simply supported $[\theta_4/-\theta_4]_s$ Gr/Epoxy plate are shown in Fig. 4.4. A uniform 8 by 8 finite element mesh was again used to model the plate. The modes are identified with their mode shape at $\theta=0$. The plate is rather thin ($\alpha/h=100$), therefore, the predictions with both DLDT and CLDT finite elements were expected to be similar. Yet, the DLDT element resulted in higher predictions of damping with respect to the CLDT element, as a result of the additional shear contributions. The difference in damping predictions, which indicates the contributions of shear damping, increased with the order of the mode. It seems that the interlaminar shear damping contributions are slightly higher for fiber orientations around $\pm 45°$, which corresponds to lay-ups with higher interlaminar shear stresses, indicating the advantage of DLDT in representing interlaminar shear damping.

To investigate further the dependence of interlaminar shear damping on the laminate lay-up, the modal damping of the previous 3 modes is shown in Fig. 4.5 for plates of various thickness. The damping predictions of the CLDT model, which are independent of thickness, are also plotted. The corresponding natural frequencies are shown in Fig. 4.6. Keeping in mind that the difference between DLDT and CLDT results indicate the magnitude of shear damping, there is definite coupling between laminate lay-up and thickness, especially in the second and third mode. The interlaminar shear damping is again higher at ±45 degs. where the interlaminar stresses are highest. In this manner, the results provide additional confidence and value to the damping mechanics.

4.4. $[\theta_5/-\theta_5]_s$ Cantilever Composite Beams

Figs. 4.7 to 4.9 present the predicted fundamental modal damping and natural frequency of $[\theta_5/-\theta_5]_s$ cantilever beams of thickness aspect ratios (l/h) 60, 30, and 15 respectively. The width and thickness of the beams were 25.4 mm (1 in) and 0.508 mm (0.2 in) respectively. The same uniform mesh consisting of 15 by 4 element subdivisions was used in all cases. For ply angles between 0 and 60 degs., the DLDT model yielded significantly higher predictions of damping and lower predictions of natural frequency in the cases of thicker beams (l/h=15). These differences were attributed to the high interlaminar stresses at the higher thickness beams. The coupling between lay-up and thickness of the beam is also illustrated in Fig. 4.9. The results demonstrate again the quality of the method in predicting shear effects due to thickness, laminate lay-up, or combinations of both.

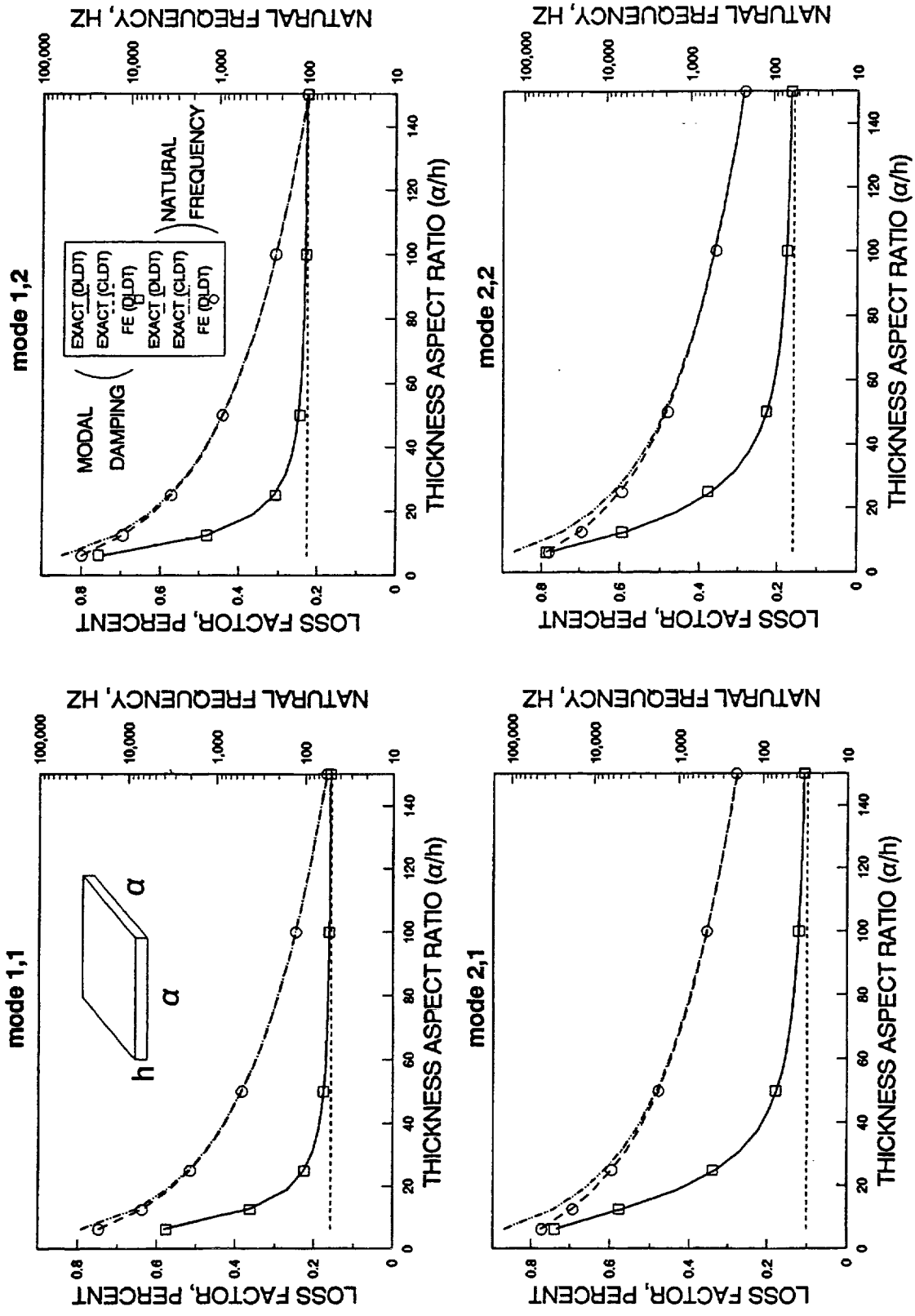

Fig. 4.1 Modal characteristics of a $[0_4/90_4]_s$ Gr/Epoxy simply-supported plate.

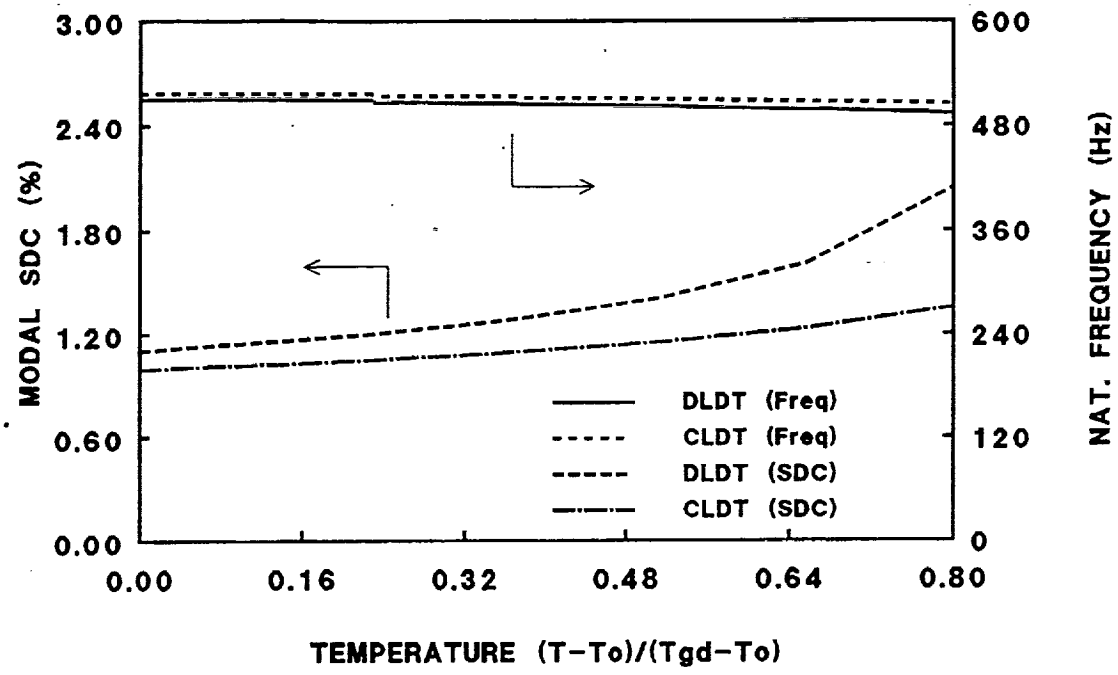

(A)

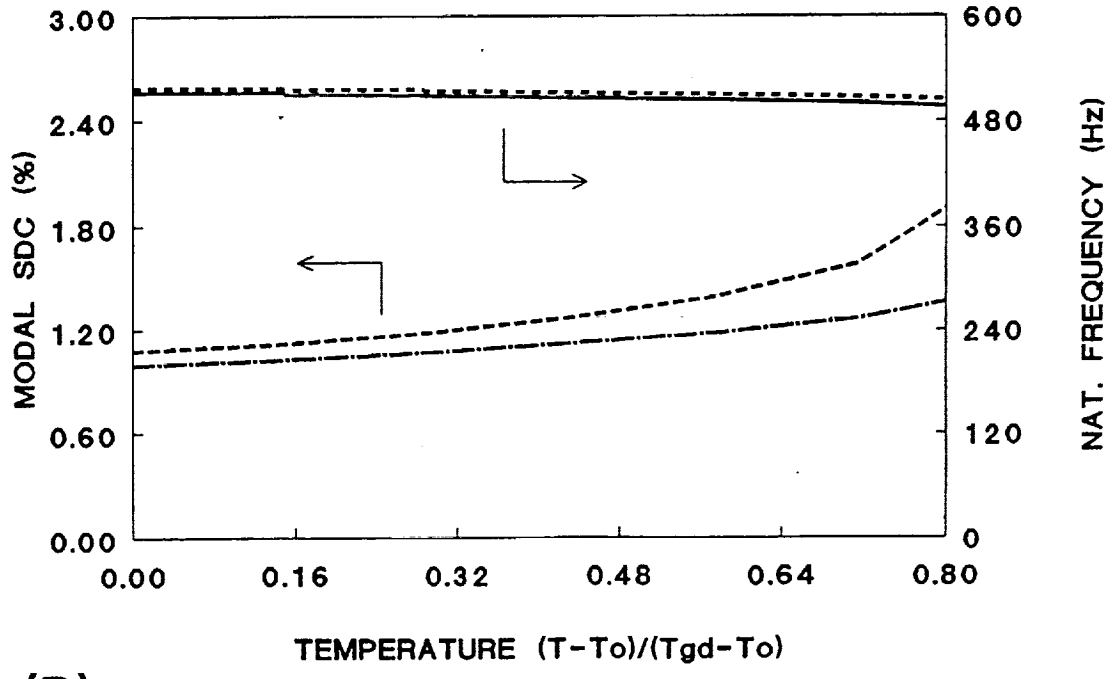

(B)

Fig. 4.2 Effect of temperature on the fundamental modal properties of square HM-S/epoxy plates. (a) $(0_4/90_4)_s$; (b) $(0/90)_{4s}$.

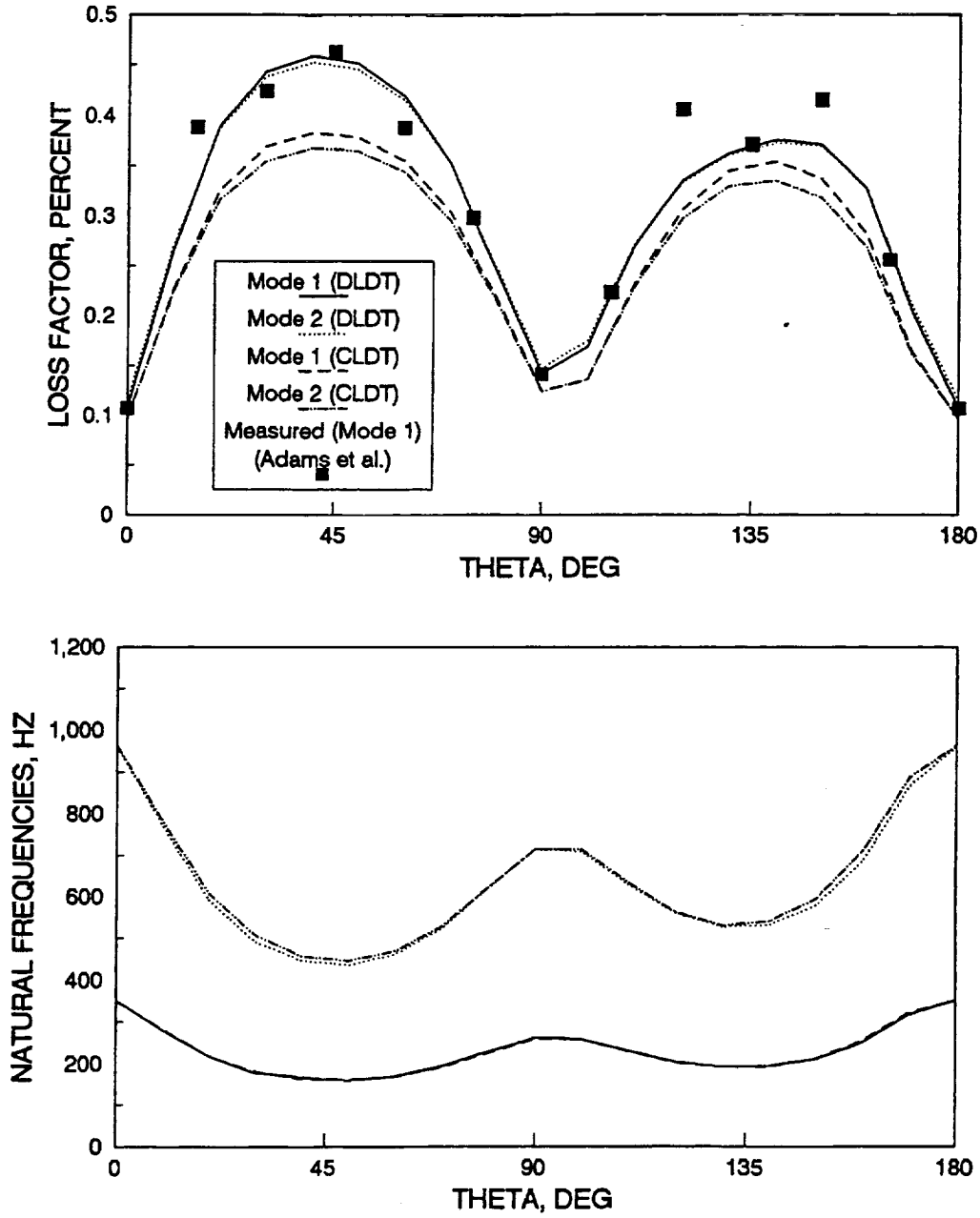

Fig. 4.3 Modal characteristics of a $[\theta/90+\theta/45+\theta/-45+\theta]_s$ cantilever beam (l/h=125; l=8 in). First and second bending modes.

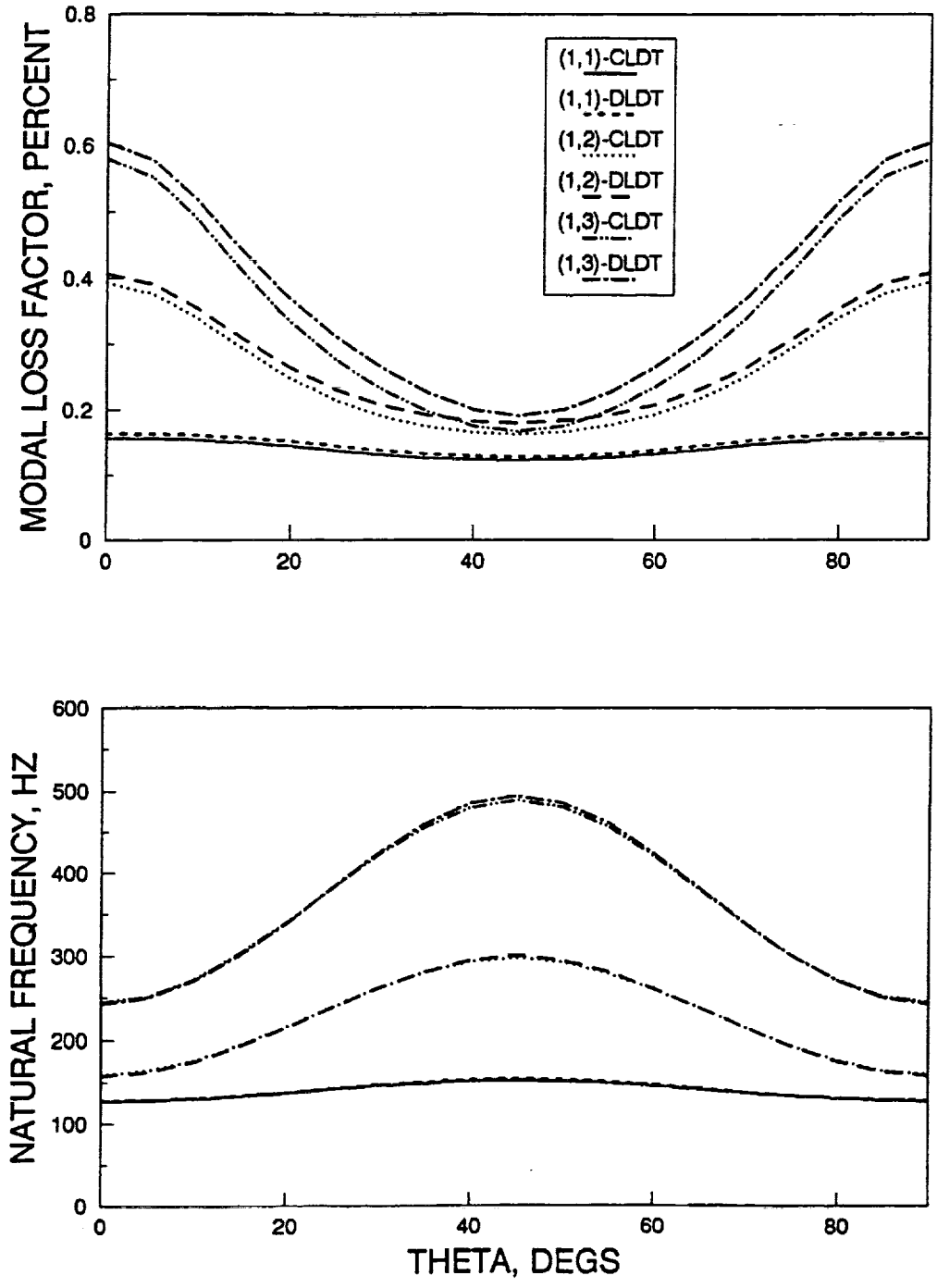

Fig. 4.4 Modal characteristics of a $[\theta_4/-\theta_4]_s$ Gr/Epoxy simply-supported plate. ($\alpha/h=100$)

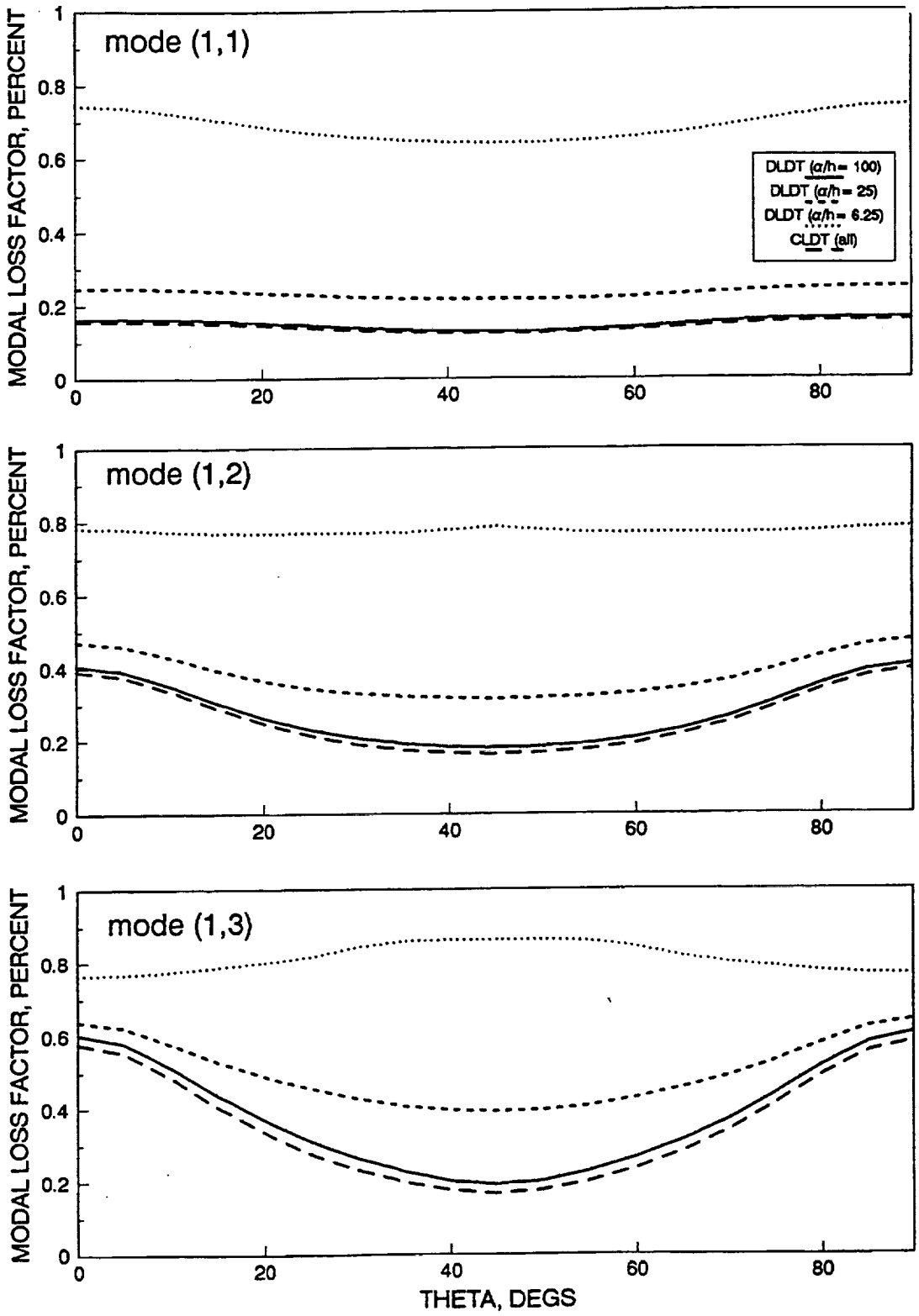

Fig. 4.5 The effect of thickness aspect ratio on the modal damping of $[\theta_4/-\theta_4]_s$ Gr/Epoxy simply-supported plate.

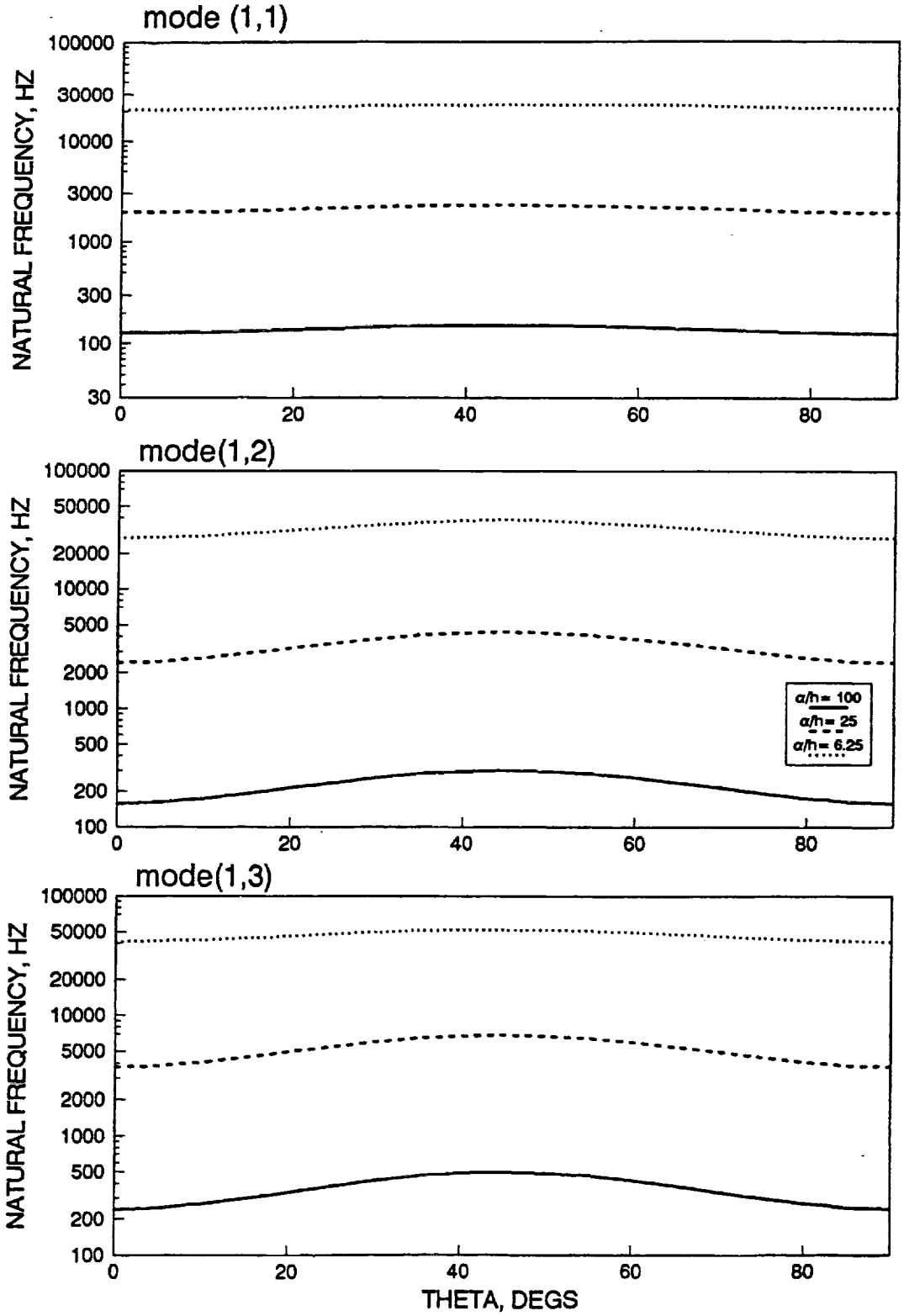

Fig. 4.6 The effect of thickness aspect ratio on the natural frequencies of $[\theta_4/-\theta_4]_s$ Gr/Epoxy simply-supported plate.

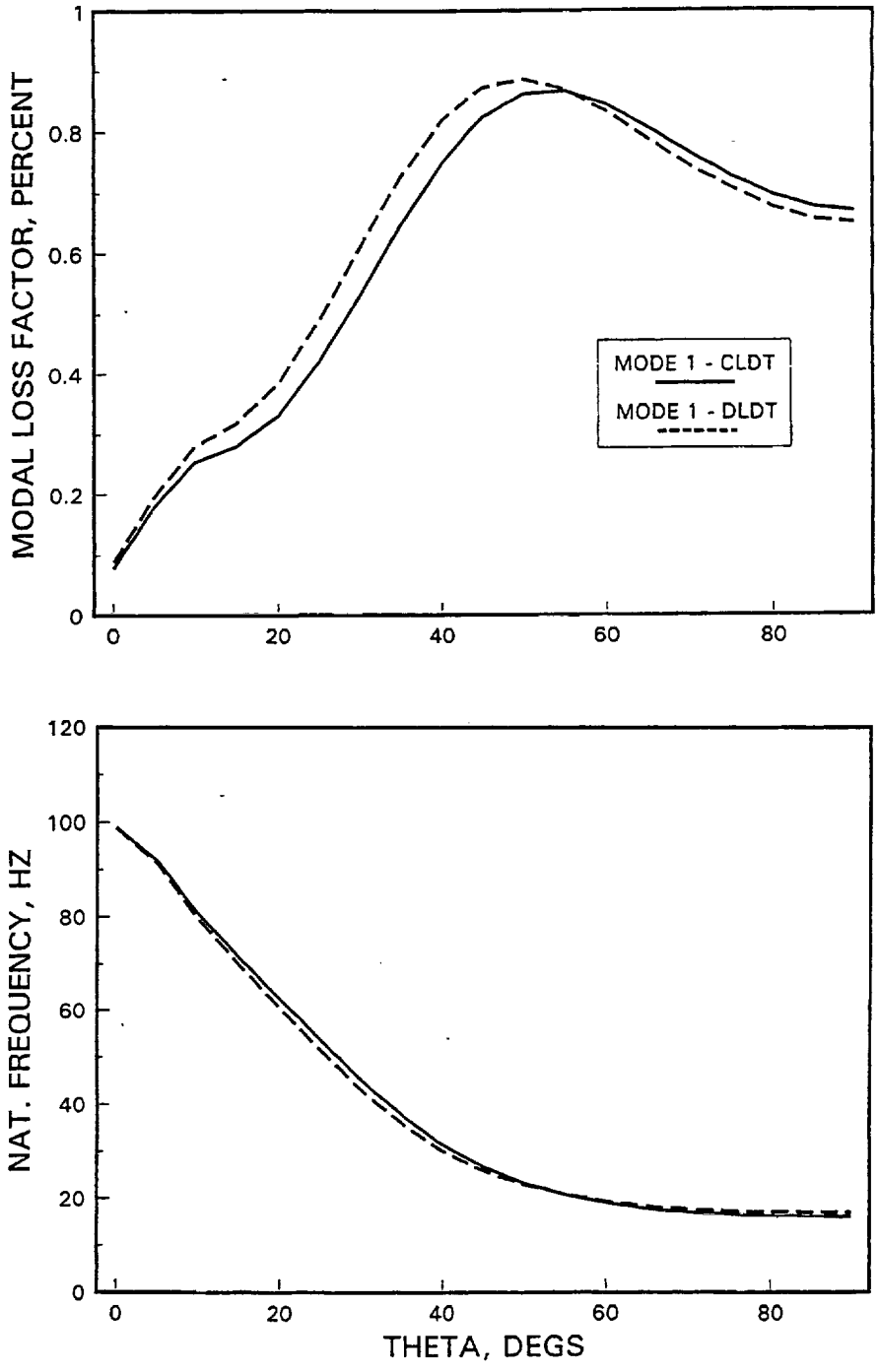

Fig. 4.7 Fundamental modal characteristics of a $[\theta_5/-\theta_5]_s$ Gr/Epoxy cantilever beam (l/h= 60).

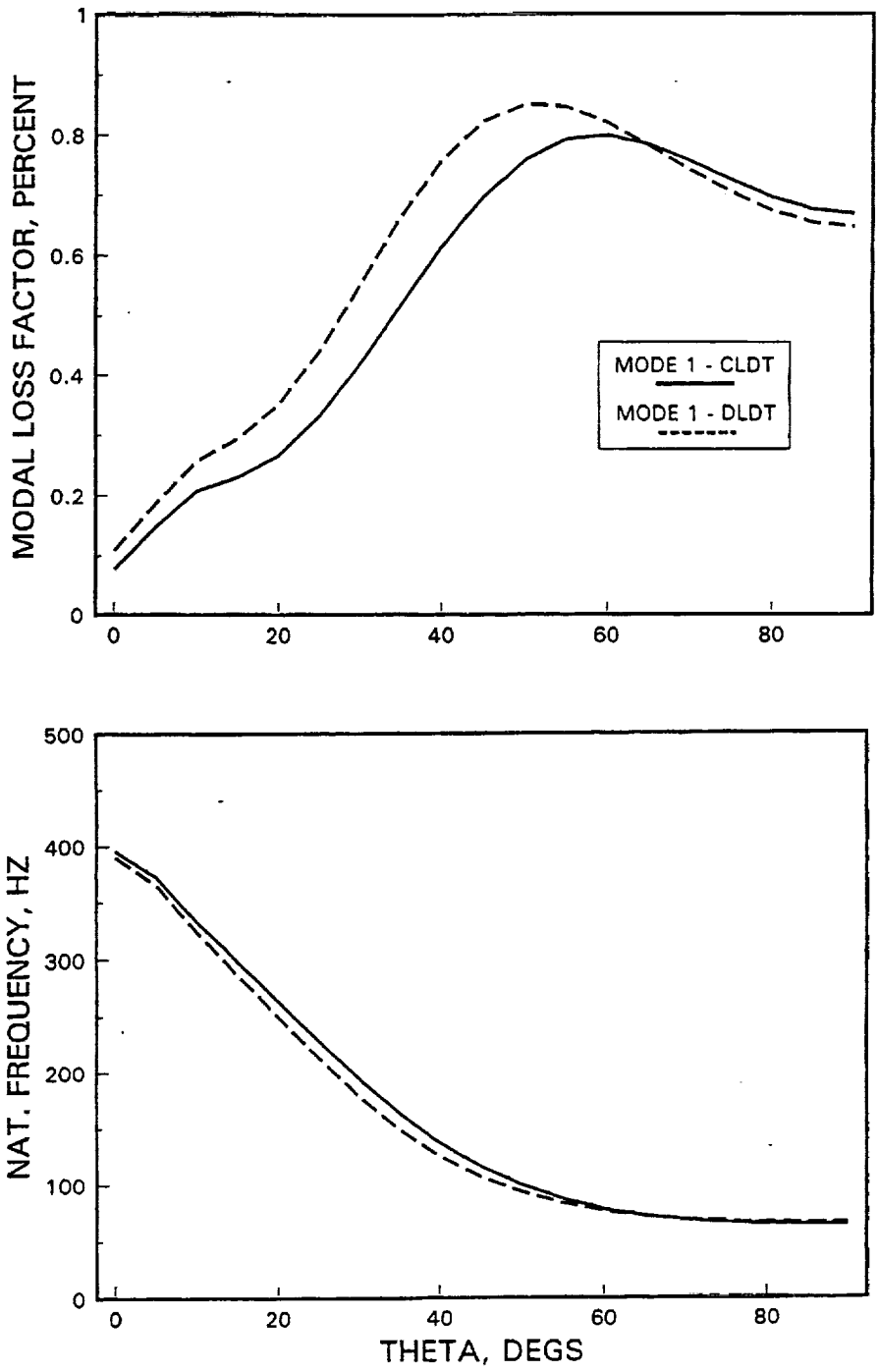

Fig. 4.8 Fundamental modal characteristics of a $[\theta_5/-\theta_5]_s$ Gr/Epoxy cantilever beam (l/h= 30).

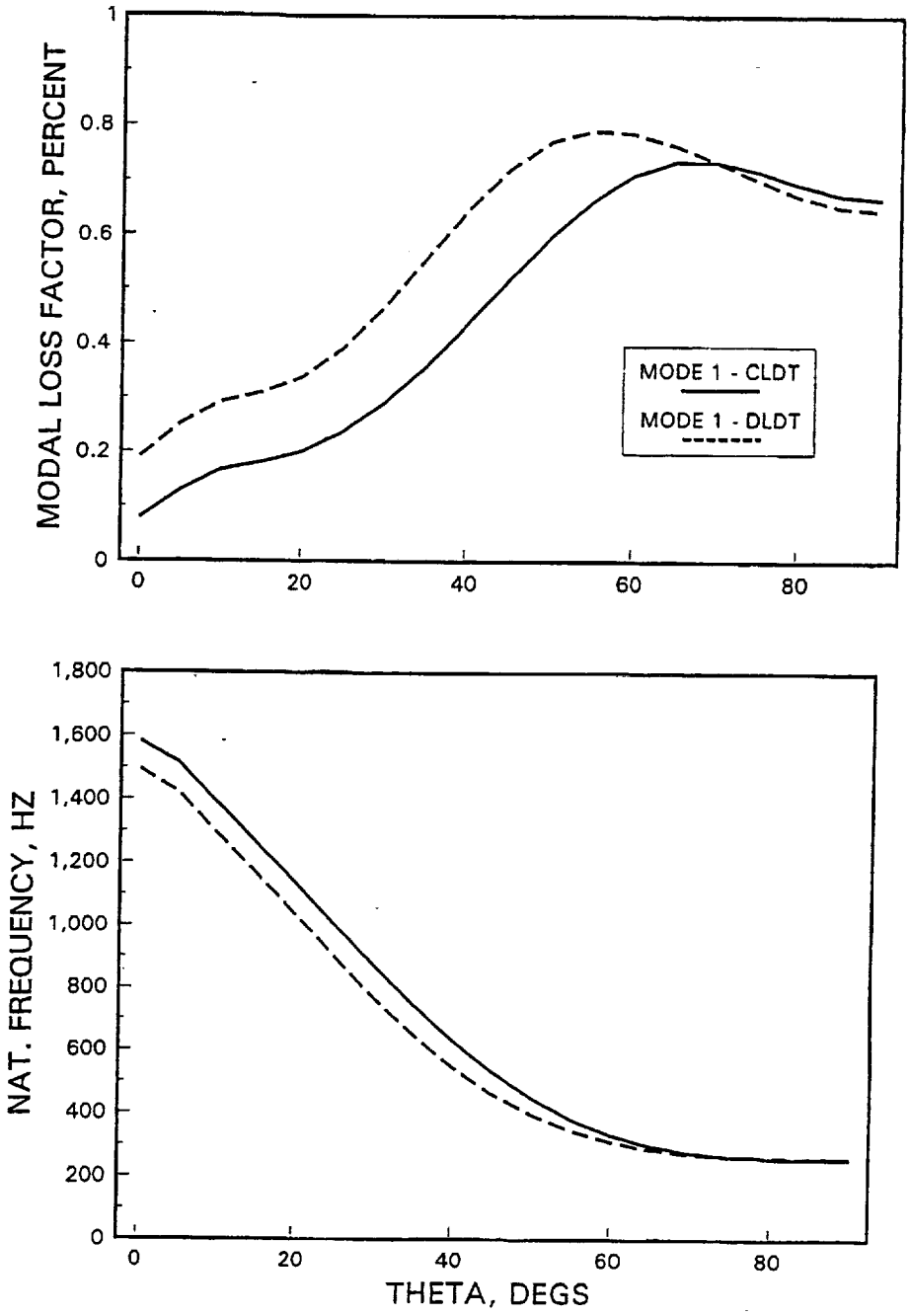

Fig. 4.9 Fundamental modal characteristics of a $[\theta_5/-\theta_5]_s$ Gr/Epoxy cantilever beam. (l/h= 15)

5. COMPOSITE PLATES WITH EMBEDDED COMPLIANT DAMPING LAYERS

5.1. Experimental Correlations

To validate the accuracy of the method and experimentally verify the effects of damping layers on the dynamic response of composite plates, a composite plate with interlaminar damping was fabricated in-house and tested in-house[1] (see Fig. 5.1). The plate was 11 in by 11 in (28 cm by 28 cm) and consisted of plies of 0.6 FVR T300/934 Graphite/Epoxy, combined with layers of ScotchDamp ISD110 damping film (3M Corp., St. Paul, MN), laid up in a $[0_2/90_2/i/90_2/0_2]s$ configuration, where i denotes the damping layer. The shear loss factor and moduli of the damping polymer, as approximated with eqs. (24) and (25), are shown in Fig. 5.2 for the frequency range of interest, and represent average values of the polymer at 30° C provided in the manufacturer's data sheet. The nominal thicknesses of the Gr/Ep tape and damping layers were 0.006 in (0.15 mm) and 0.005 in (0.13 mm), respectively. The plate was laid up by hand, co-cured at 350° F (175° C) and 50 psi (345 KPa), and finally cut to size.

Frequency response functions for the composite plate were obtained from impulse tests. A special fixture with "knife-edge" supports was designed to support as closely as possible the plate in the SS configuration described by eqs. (16), and to minimize the friction forces. The plate was impacted at the quarter point $(x/\alpha, y/\beta)= (0.25, 0.25)$ with an instrumented hammer, and the acceleration was measured with a miniature accelerometer (1 gm mass) at points $(x/\alpha, y/\beta)= (0.5, 0.5)$ and $(x/\alpha, y/\beta)= (0.25, 0.75)$. The signals from the hammer and the accelerometer were recorded with a high speed digital data acquisition system, and was then processed using FFT software to obtain the frequency response functions of the plate. The accelerance of the plate at the previously mentioned points is shown in Fig. 5.3.

The predicted response was synthesized from the calculated modal damping and natural frequencies using a modal superposition technique (Fig. 5.3) with frequency effects included as described in the previous section. With the exception of the first mode, the predicted response reproduces sufficiently the measured one. The mismatch and higher damping of the first mode was also observed in the test of a monolithic aluminum plate, hence, it was attributed to imperfections in the experimental supports. There is some underestimation of the damping in the predicted response, which may be attributed to friction and air damping present in the experiment. However, both predicted and measured results fall within the

[1] The author wants to thank Mr. Peter Addente for fabricating the composite plates and Dr. Michael J. Pereira for testing the plates. Their contributions are gratefully acknowledged.

range of uncertainty predicted from the upper and lower bounds of scatter in the manufacturer's data for this polymer film damping. The agreement is improved at higher modes, because the effects of the supports are less dominant compared to the shear damping contributions of the damping material.

5.2. Parametric Studies

This section presents applications of the developed methodology on square laminated Gr/epoxy simply-supported (SS) plates with interlaminar damping layers. The dimensions of the plate were assumed 11.8 in by 11.8 in (30 cm by 30 cm). The composite material was HM-S graphite/epoxy with elastic and damping properties given in ref. 6. Unless otherwise stated, the fiber volume ratio (FVR) of the composite plies were 0.50. The shear modulus and shear loss factor of the interlaminar damping layer were 0.9 kpsi (6.2 MPa) and 1.02 respectively, and represent average values of a typical commercial damping polymer (ScotchDamp ISD112, 3M Corp)[16] at room temperature. Experimental data regarding the normal loss factor and Young's Modulus of the damping polymer was not available. Because the present theory includes provisions for normal damping and modulus, a Poisson's ratio equal to 0.3 and a very low normal loss factor (0.016) were assumed for the damping polymer to ensure minimal contribution on the damping of the plate. This assumption was further reinforced by parametric studies which quantified the insensitivity of the modal characteristics (natural frequencies and damping) of the plate to the normal damping and the Poisson's ratio of the damping layer. The effects of frequency on the properties of the damping polymer were neglected here, in order to isolate the effects of composite anisotropy and inhomogeneity on the performance of the damping layers. The nominal thickness t_i of the damping layer was equal to the typical thickness of a composite ply $t_i = 0.005$ in (0.13 mm). In all cases a concentrated vertical load of 100 lbs (445 N) was applied at the center of the plate. Linear interpolation functions $F^j(z)$ were used to calculate the in-plane displacements through-the-thickness of the laminate.

The ply-stacking sequence is represented using the traditional convention, but interlaminar damping layers of thickness t_i are identified with symbol *i*. For comparison purposes, calculated results for aluminum plates are also presented, in such case, an aluminum layer of thickness equal to the thickness of k plies will be identified as Al_k. All laminate configurations were symmetric. The modal loss factor is normalized by the shear loss factor of the polymer, and will be referred in the next paragraphs as normalized modal damping.

Predicted modal damping, natural frequencies, and static deflections at the center of an aluminum $(Al_4/i/Al_4)s$ and various Gr/epoxy damped plates, $(0_4/i/0_4)s$, $(0_4/i/90_4)s$ and

$(0_2/90_2/i/0_2/90_2)s$ are shown in Table 5.1. All plates have high modal damping values. The laminates with the higher anisotropy in the composite sublaminates, ie. $(0_4/i/0_4)s$ and $(0_4/i/90_4)s$, exhibit the higher damping in the fundamental mode. The $(0_4/i/90_4)s$ laminate exhibits the higher anisotropy variation through-the-thickness among all plates, and this seems to have resulted in some higher modal damping values. Interestingly, this laminate has comparable static stiffness and natural frequency with the $(0_2/90_2/i/0_2/90_2)s$ laminate, which illustrates the possibility for higher damping values in some modes without significantly penalizing other structural characteristics. The high damping of the unidirectional composite laminate was attributed in part to the lower stiffness of the plate. The composite plates have higher static deflections but lower areal density than the aluminum plate, as a result, they exhibit slightly higher fundamental frequencies. The damping of the higher modes varies widely and depends on the respective mode shape. The variation is more predominant for the composite plates.

The variations of the first modal damping, natural frequency, and static deflection at the center of the plate are plotted in Fig. 5.4 as functions of the damping layer thickness. The thickness of the composite sublaminates was kept constant, therefore, the total laminate thickness was varied. The layer thickness t_i is normalized by the nominal ply thickness t_1= 0.005 in. For layer thicknesses in the range of practical interest, the laminate with the higher anisotropy through-the-thickness $(0_4/i/90_4)s$ provides consistently higher damping than the aluminum $(Al_4/i/Al_4)s$ and $(0_2/90_2/i/0_2/90_2)s$ laminates. This results are consistent with the expectation that composite laminates will induce higher interlaminar shear stresses in the interlaminar layer, in order to balance the elastic anisotropy and nonuniformity of adjacent plies, as opposed to traditional isotropic laminates where interlaminar stresses will only balance the bending stresses through-the-thickness. For all laminates, the modal damping increased with thickness and tends to reach a maximum at higher thickness values. It was observed that for plates of lower aspect ratio α/h the peak in the modal damping shifts towards lower thicknesses. Finally, it seems that a critical damping layer thickness exists (in this case approximately equal to the ply thickness), such that, damping layers with less or equal thickness will add low but significant damping with negligible effects on the structural properties (static deflection, natural frequency).

Fig. 5.5 shows the predicted variations of modal damping, natural frequency and static deflection with the aspect-ratio of the plate (α/h). As was expected, the modal damping of all plates increases at lower aspect ratios because shear prevails over flexure. Interestingly, the damping reaches a peak at very low aspect ratios and then decreases again. Intuitively, at very low aspect ratios through-the-thickness deformations will gradually prevail over shear and the effectiveness of the damping layer will be decreased. Nevertheless, the kinematic assumptions of the DLDT are not expected to be valid at the regime of very low aspect ratios because the present approach assumes negligible through-the-thickness strains. Both

natural frequency and static stiffness consistently increase with lower aspect ratios.

Fig. 5.6 presents the variation of modal damping, natural frequency, and static deflection as functions of the FVR of the inner and outer composite sublaminates with respect to the damping layers. Fig. 5.6 demonstrates one unique advantage of composite laminates, that is, the additional tailoring capacity they can introduce. In both laminates, the FVR variation of the outer sublaminate has a definite effect on the modal damping of the plate. The damping increases almost linearly with the FVR, indicating that the most important composite parameter is the longitudinal modulus. Since both natural frequency and static stiffness also increase with the FVR of the outer sublaminate, the obvious choice is to have outer sublaminates of very high FVR. The modal damping is less sensitive to FVR variations of the inner sublaminate, and decreases slightly with FVR.

Table 5.1. Static and dynamic characteristics of composite plates with interlaminar layers. (t_i=0.005 in; numbers in parenthesis indicate mode order)

	$(Al_4/i/Al_4)s$	$(0_4/i/0_4)s$	$(0_4/i/90_4)s$	$(0_2/90_2/i/0_2/90_2)s$
Areal Density, 10^{-3} lb/in^2				
	7.95	4.92	4.92	4.92
Static Deflection (Center), in				
	0.334	0.604	0.496	0.456
Normalized Modal Damping				
Mode 1	0.131 (1,1)	0.153 (1,1)	0.153 (1,1)	0.098 (1,1)
2	0.259 (1,2)	0.126 (1,2)	0.066 (1,2)	0.266 (1,2)
3	0.259 (2,1)	0.104 (1,3)	0.433 (2,1)	0.252 (2,1)
4	0.346 (2,2)	0.110 (1,4)	0.355 (2,2)	0.277 (2,2)
5	0.374 (1,3)	0.370 (2,1)	0.033 (1,3)	0.438 (1,3)
6	0.374 (3,1)	0.355 (2,2)	0.218 (2,3)	0.395 (2,3)
7	0.415 (2,3)	0.319 (2,3)	0.598 (3,1)	0.381 (3,1)
8	0.415 (3,2)	0.134 (1,5)	0.553 (3,2)	0.380 (2,3)
9	0.448 (1,4)	0.277 (2,4)	0.028 (1,4)	0.545 (1,4)
10	0.448 (4,1)	0.249 (2,5)	0.438 (3,3)	0.418 (3,3)
Natural Frequencies, Hz				
Mode 1	115.7	119.9	119.9	124.0
2	265.0	152.7	211.8	272.6
3	265.0	230.1	354.8	357.7
4	395.2	351.2	402.4	437.7
5	474.5	383.4	409.3	495.2
6	474.5	402.3	541.7	606.7
7	585.6	447.7	635.2	688.7
8	585.6	508.7	667.9	736.7
9	722.5	531.4	697.6	747.2
10	722.5	656.5	766.7	851.6

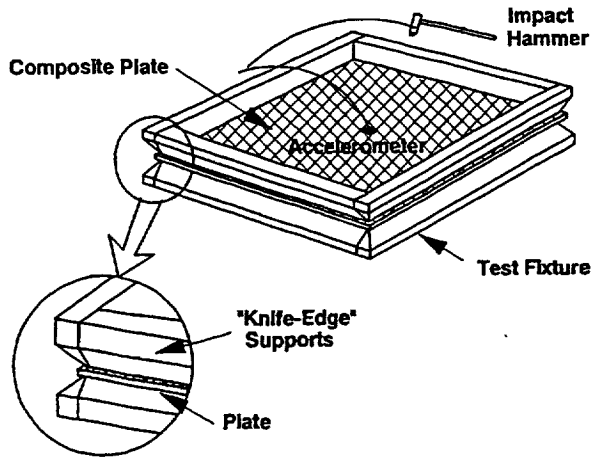

Fig. 5.1 Experimental configuration showing composite plate in knife-edge supports.

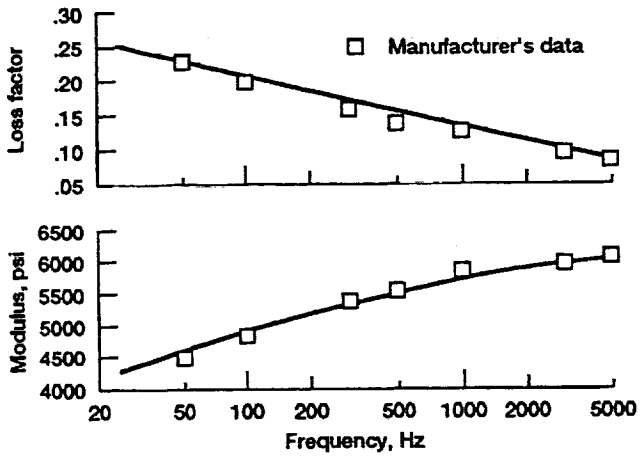

Fig. 5.2 Mechanical properties of the ISD110 damping polymer at 30° C. Shear modulus and shear loss factor.

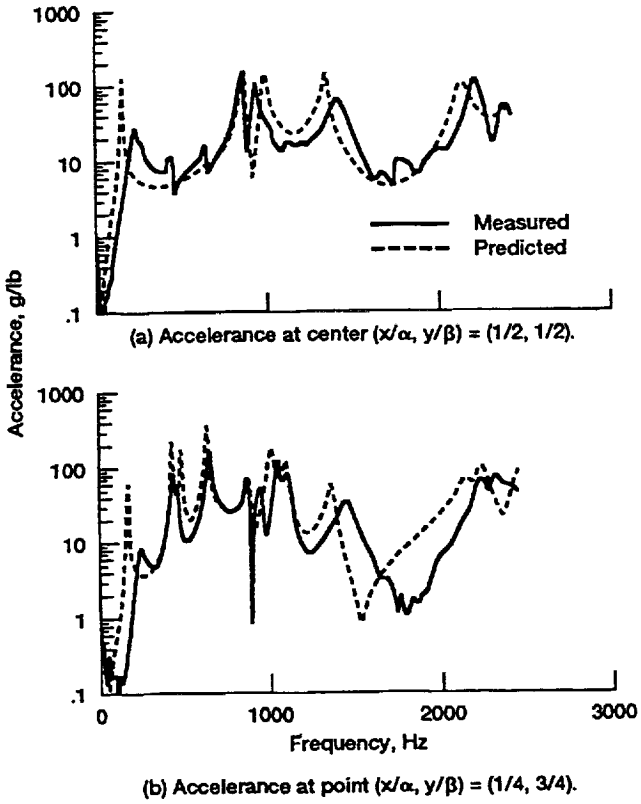

Fig. 5.3 Frequency response of a $(0_2/90_2/i/90_2/0_2)s$ T300/934 plate with ISD110 damping layers.

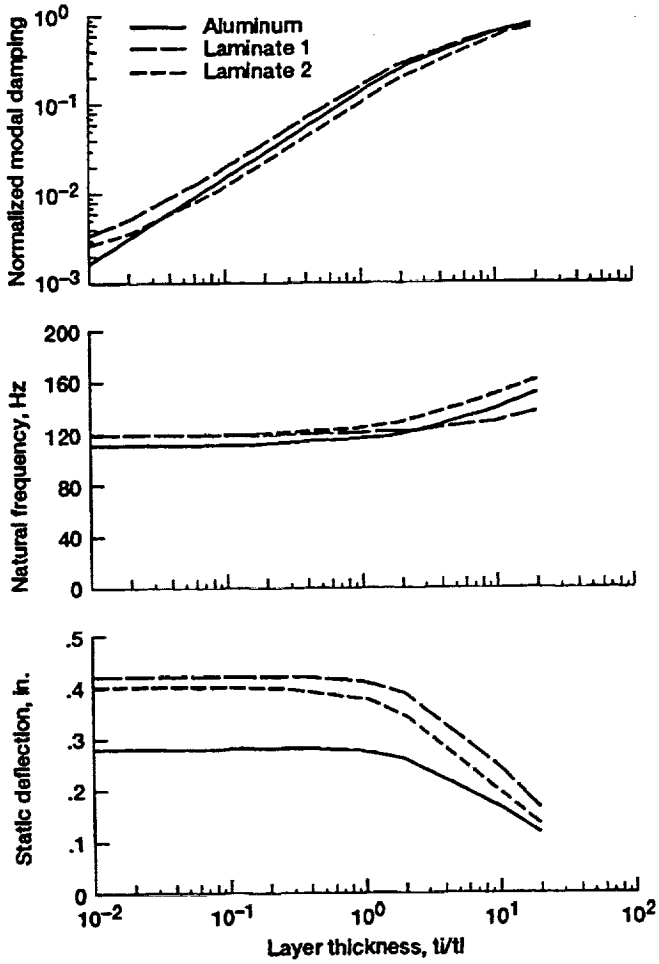

Fig. 5.4 Effect of damping layer thickness. Alum.= $(Al_4/i/Al_4)s$; Lam. 1= $(0_4/i/90_4)s$; Lam. 2= $(0_2/90_2/i/0_2/90_2)s$

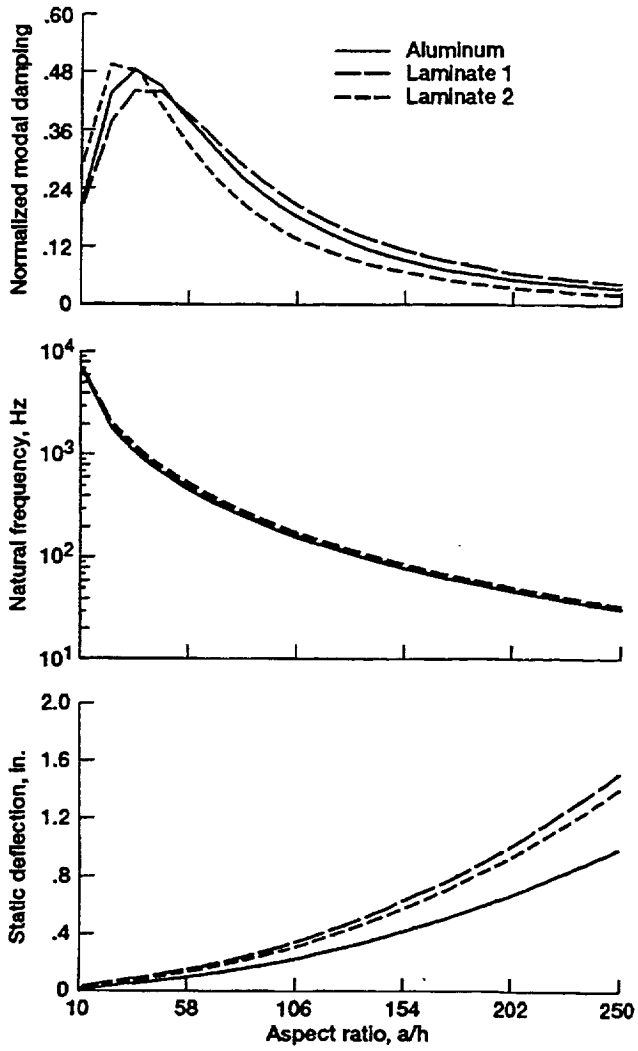

Fig. 5.5 Effect of plate aspect ratio. Alum.= $(Al_4/i/Al_4)s$; Lam. 1= $(0_4/i/90_4)s$; Lam. 2= $(0_2/90_2/i/0_2/90_2)s$

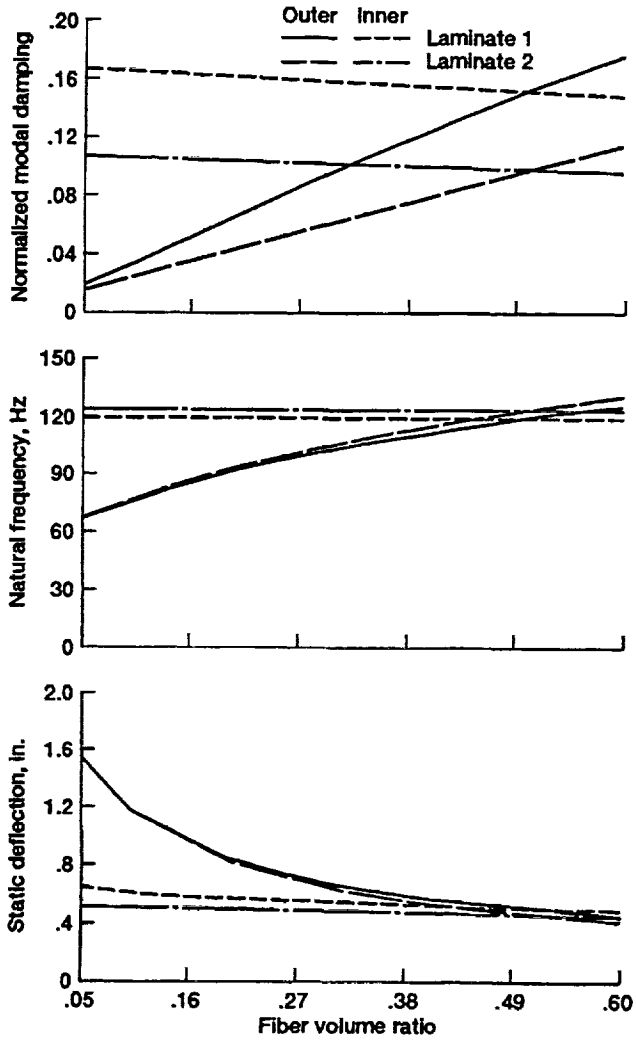

Fig. 5.6 Effect of fiber volume ratio. Laminate 1= $(0_4/i/90_4)s$; Laminate 2= $(0_2/90_2/i/0_2/90_2)s$

6. DAMPING ENHANCEMENT IN SPECIALTY COMPOSITE STRUCTURES

The developed structural damping mechanics were also applied on the analysis of damping in various composite plates with embedded compliant interlaminar damping layers. The objectives of the case studies were: (1) to further evaluate the quality of method by correlating predictions with both analytical and experimental results; and (2) to explore and quantify unique advantages in improving the vibroacoustic characteristics of composite structures by embedding compliant layers between plies with strong interlaminar inhomogeneity. These applications demonstrate the potential to engineer/tailor such specialty composite laminates for high dynamic performance.

The selected materials were 0.60 FVR T300/934 composite, and ScotchDamp ISD110 damping film (3M Corp., St. Paul, MN) as interlaminar layers. The shear modulus and shear loss factor of the damping polymer were assumed 5.5 kpsi and 0.16 respectively, and they represent average values of the polymer at 500 Hz and 30° C as provided by the manufacturer's data sheet. Due to non-existing data, the Young's modulus of the damping polymer was assumed 15.4 kpsi and the normal loss factor was assumed to be negligible (0.016). Parametric studies have indicated strong insensitivity of modal damping and frequency to the dilatational properties of the damping polymer. The damping properties of the 934 epoxy were assumed equal to typical damping values of epoxy matrices. Unless otherwise stated, the nominal thicknesses of the Gr/Ep plies and damping layers were 0.0058 in (0.15 mm) and 0.005 in (0.13 mm), respectively.

6.1. $[0_4/i/90_4]s$ Simply Supported Plate.

The quality and accuracy of the developed structural damping mechanics were first investigated by comparisons with exact analytical solutions. Fig. 6.1 shows the modal damping and natural frequencies of a $[0_4/i/90_4]s$ simply supported plate predicted by the discrete finite element method and the exact plate solutions developed based on the discrete laminate damping theory [10]. The finite element analysis involved an 8 by 8 uniform mesh subdivision. As seen in Fig. 6.1, there is excellent agreement between the finite element based and exact damping predictions. The accuracy of the predictions is slightly but gradually reduced at higher modes, because of the limitation of the implemented mesh in representing the higher mode shapes. A more refined mesh would readily improve the predictions at higher modes.

6.2. Angle-ply Unsupported Plates.

The predicted dynamic characteristics of two symmetric angle-ply plates with compliant damping layers are also shown in Figs. 6.2 and 6.3. The laminate configurations were $[45_2/-45_2/i/45_2/-45_2]_s$ and $[22.5_2/-22.5_2/i/22.5_2/-22.5_2]_s$ respectively. In-house experimentally measured damping values and natural frequencies for these plates at a "free-hanging" configuration are also shown in these figures. The composite plates were fabricated by hand lay-up, co-cured at 350° F (175° C) and 50 psi (345 KPa), and finally cut to 28 cm by 28 cm (11 in by 11 in).

In both cases, the correlation between measured and predicted modal damping and corresponding natural frequencies appears very good, especially in the low frequency regime. Predicted and measured results for composite plates of identical laminations but w/o damping layers are also shown in Figs. 6.2 and 6.3. It is pointed out, that the sole purpose of plotting these results is to compare and demonstrate the obtained improvements in the damping characteristics of the various plates, rather than comparing the accuracy of the method, since damping data for the composite system were not available at the time of this paper.

6.3. Angle-Ply Laminates

The predicted loss factors and corresponding natural frequencies of the first five modes of two simply-supported plates, with laminations $[\theta_2/-\theta_2/i/\theta_2/-\theta_2]s$ and $[\theta_2/-\theta_2/i/-\theta_2/+\theta_2]s$ respectively, are shown in Figs. 6.4-6.8 as functions of the ply angle θ. The modal loss factors and natural frequencies of plates with identical geometrical and laminate configurations, but without damping layers (undamped), that is $[\theta_2/-\theta_2/\theta_2/-\theta_2]s$ and $[\theta_2/-\theta_2/-\theta_2/+\theta_2]s$ respectively, are also plotted in the same Figures.

Clearly, the addition of the damping layers drastically improved the damping capacity of the composite plates. But most importantly, the predicted results demonstrate that increased through-the-thickness inhomogeneity and anisotropy in the composite sublaminates may significantly improve the damping of the composite structure. This damping enhancement is further signified by the observation that the predicted damping of the composite plates without damping layers is typically reduced for ply angles between 0 and 90°. Finally, the damped plates exhibit similar or higher natural frequencies than the undamped plates between 0 and 90 degs, hence, this enhancement of damping does not seem to reduce the natural frequencies and stiffness.

As seen in Figs. 6.4-6.8, the improvements in the damping are increased at higher modes, for example mode 1 (1,1), mode 2 (1,2), mode 3 (1,3), and mode 5 (2,2). The numbers in parenthesis indicate the mode order at $\theta=0$ degs. The damping increases, indicate the

interrelation between laminate configuration and mode shape. A significant part of the damping improvements were induced by altering the anisotropy in the restraining composite sublaminates. It seems though, that alternating fiber orientations in the plies which contain the damping layer produce some additional damping improvement. It is also interesting to note, that as the stiffness of the restraining sublaminate remains the most critical mechanism for enhancing shear damping in the interlaminar layer, not all modes will exhibit the previous damping improvements. This is illustrated in mode 4, which corresponds to mode shape (2,1) and exhibits its highest damping at $\theta=0$ degs, that is, when the outer restraining sublaminates have the higher flexural stiffness in the direction of the flexure.

The presented results, illustrated the accuracy and versatility of the structural damping mechanics in predicting the damped dynamic characteristics of specialty composite structures. The applications have also demonstrated the potential to "engineer" composite laminates with embedded interlaminar damping layers to provide higher and tailorable damping than traditional isotropic materials. The results finally demonstrate the opportunity to tailor and "engineer" composite structures for improved dynamic characteristics in terms of damping and natural frequencies.

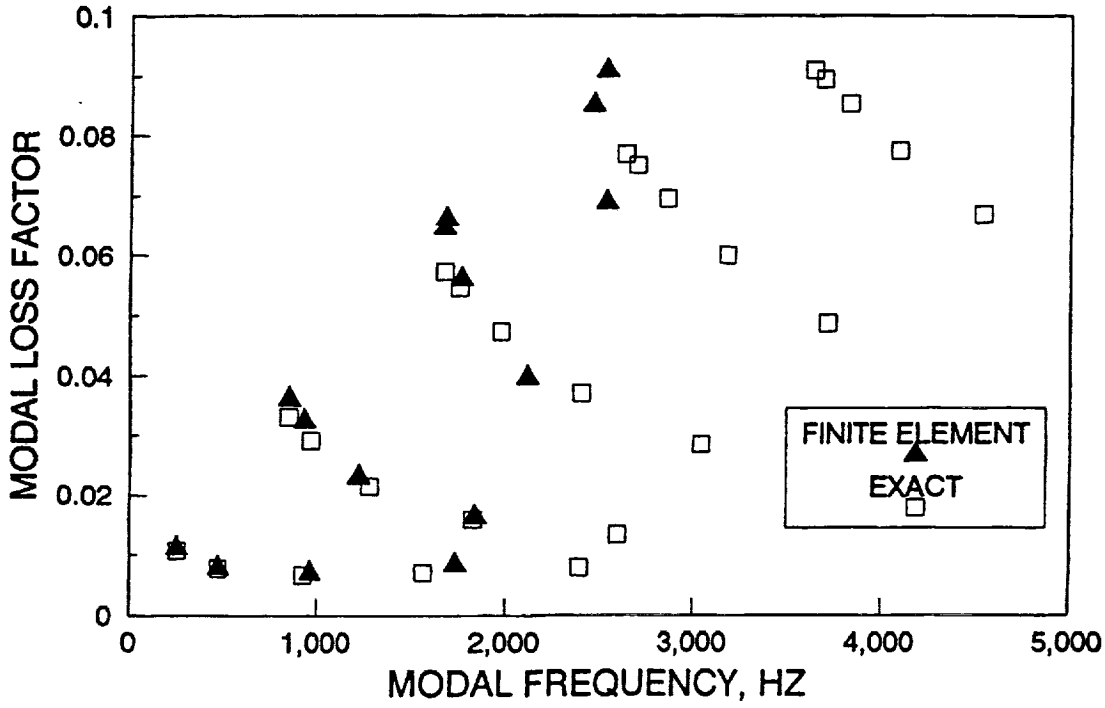

Fig. 6.1 Modal characteristics of a $(0_4/i/90_4)s$ T300/934 simply supported plate with ISD110 damping layers.

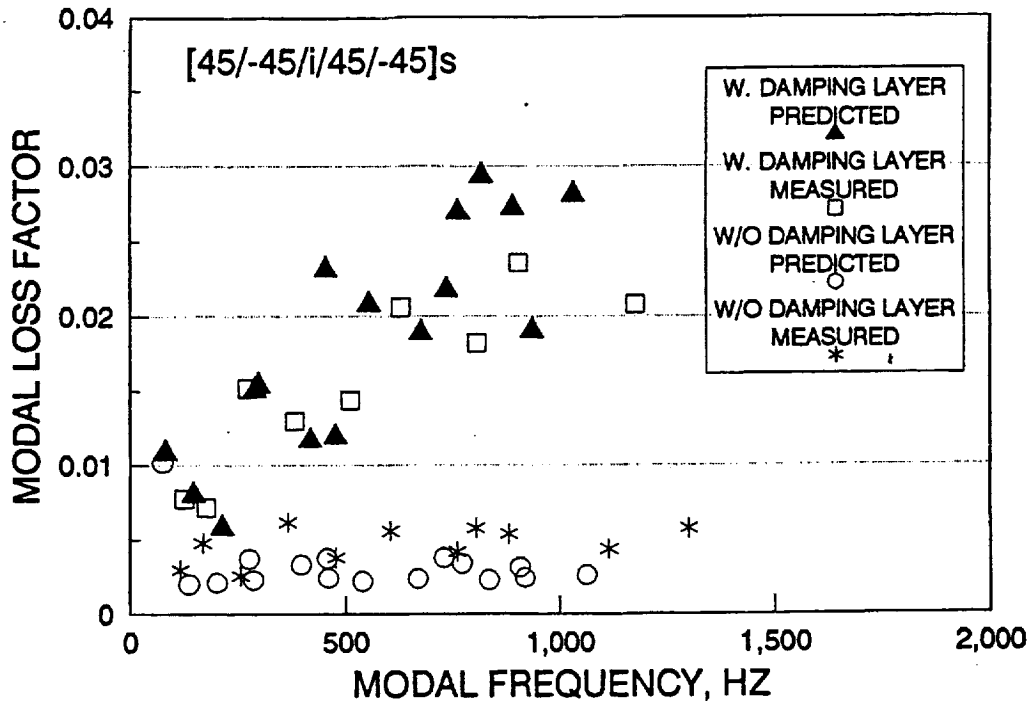

Fig. 6.2 Modal characteristics of a $[45_2/-45_2/i/45_2/-45_2]_s$ T300/934 simply supported plate with ISD110 damping layers.

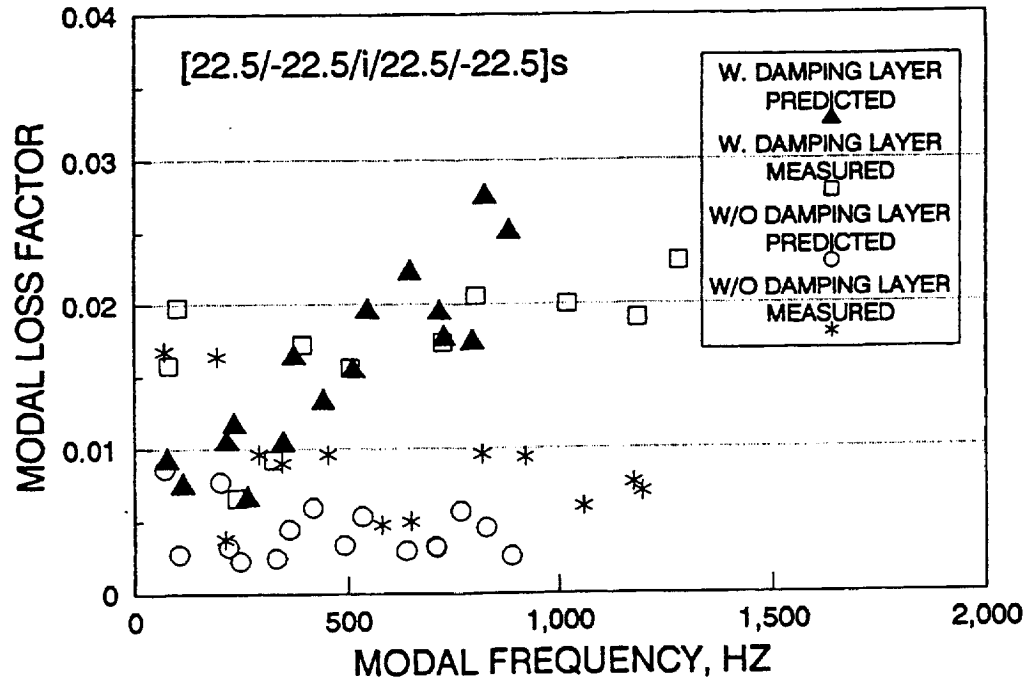

Fig. 6.3 Modal characteristics of a $[22.5_2/-22.5_2/i/22.5_2/-22.5_2]_s$ T300/934 simply supported plate with ISD110 damping layers.

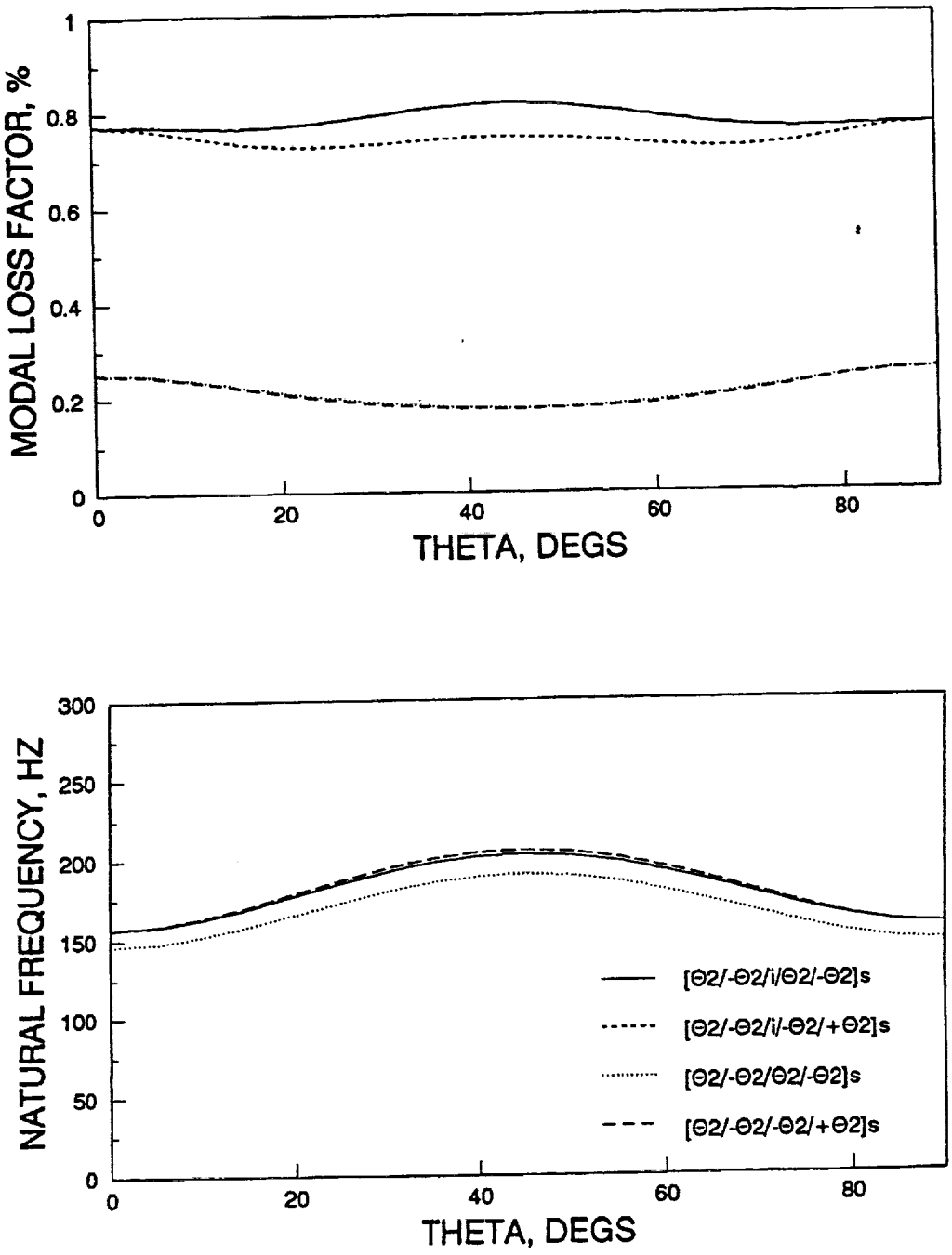

Fig. 6.4 Modal loss factor and natural frequency of angle-ply T300/934 simply supported plates; mode 1.

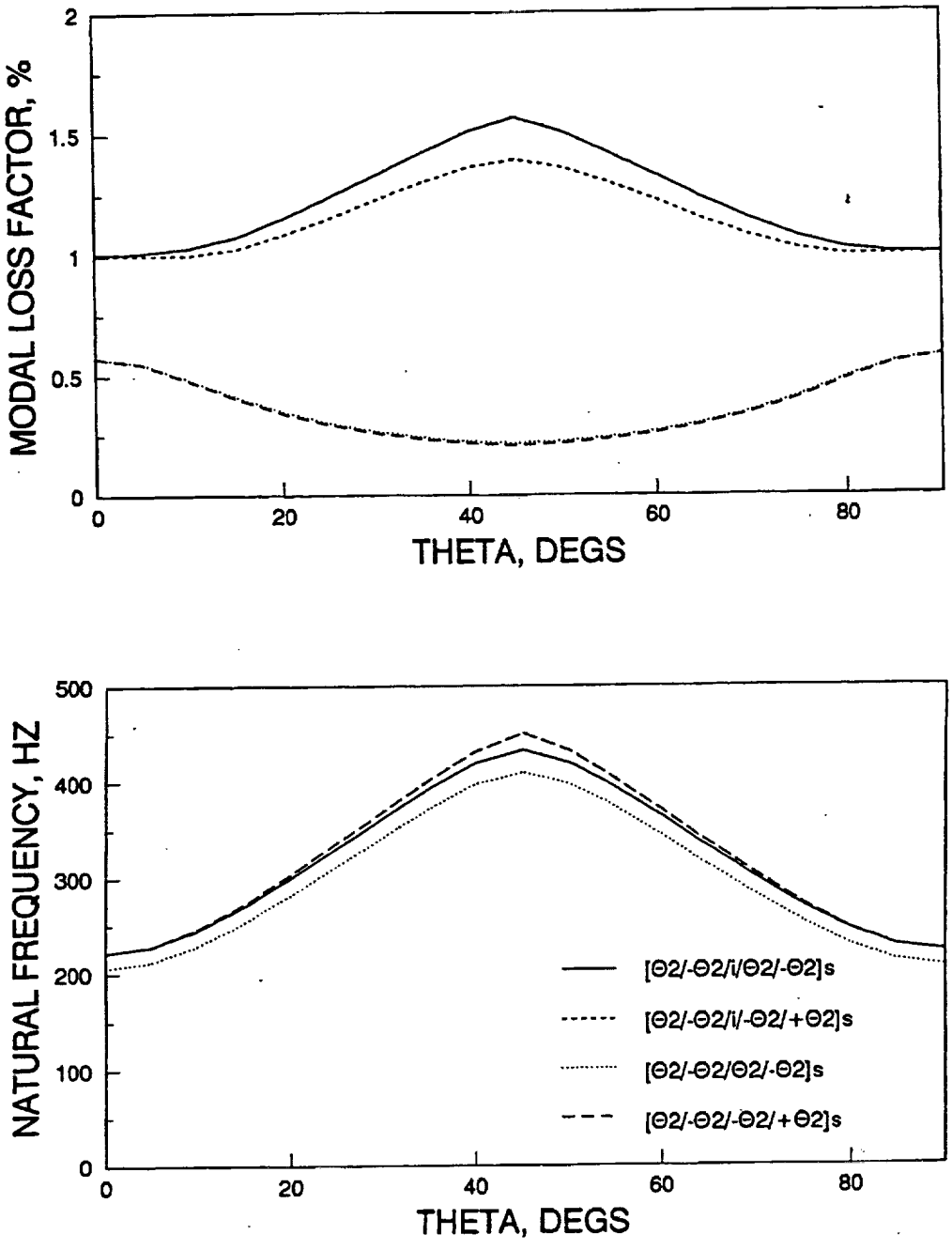

Fig. 6.5 Modal loss factor and natural frequency of angle-ply T300/934 simply supported plates; mode 2.

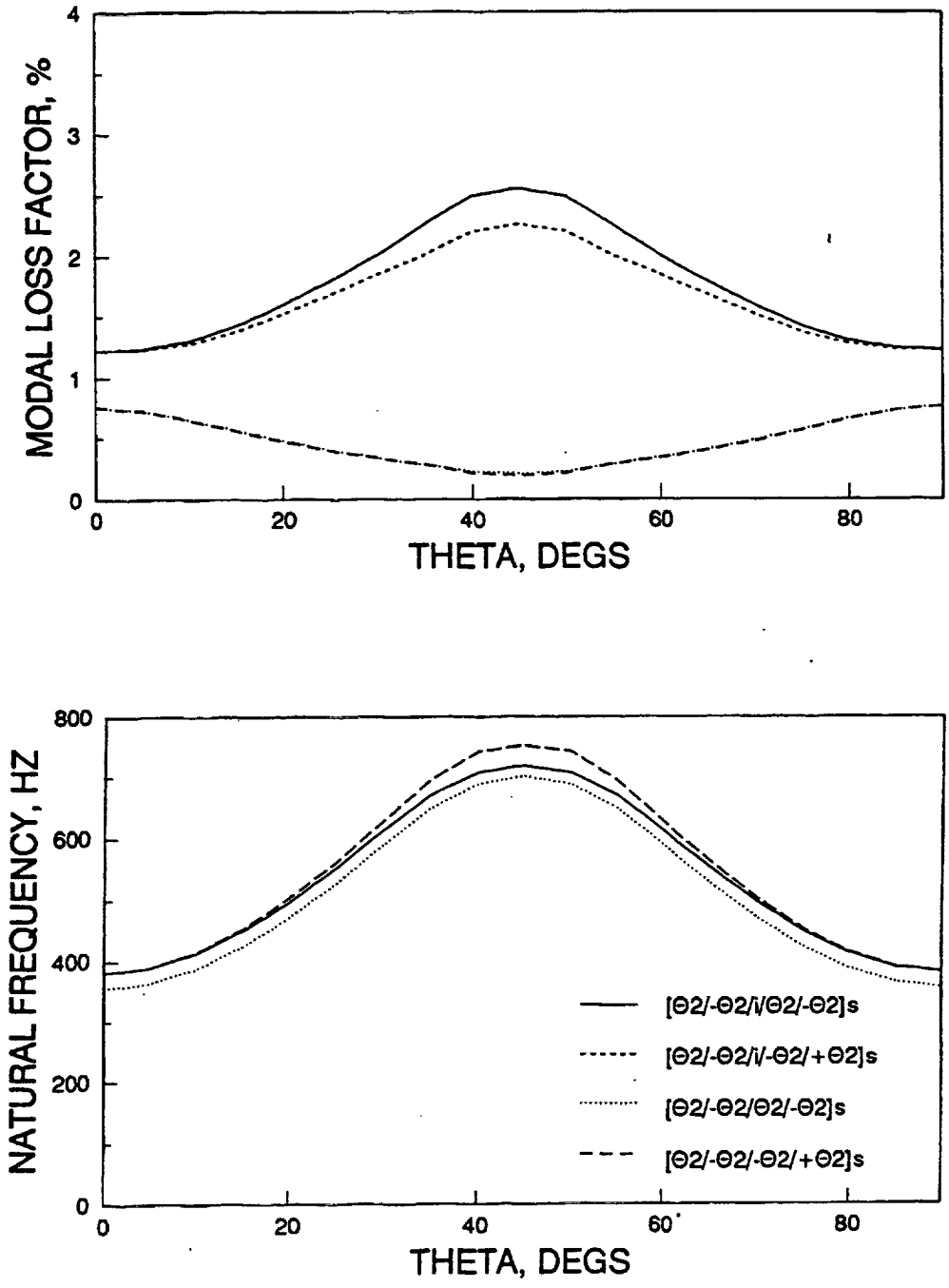

Fig. 6.6 Modal loss factor and natural frequency of angle-ply T300/934 simply supported plates; mode 3.

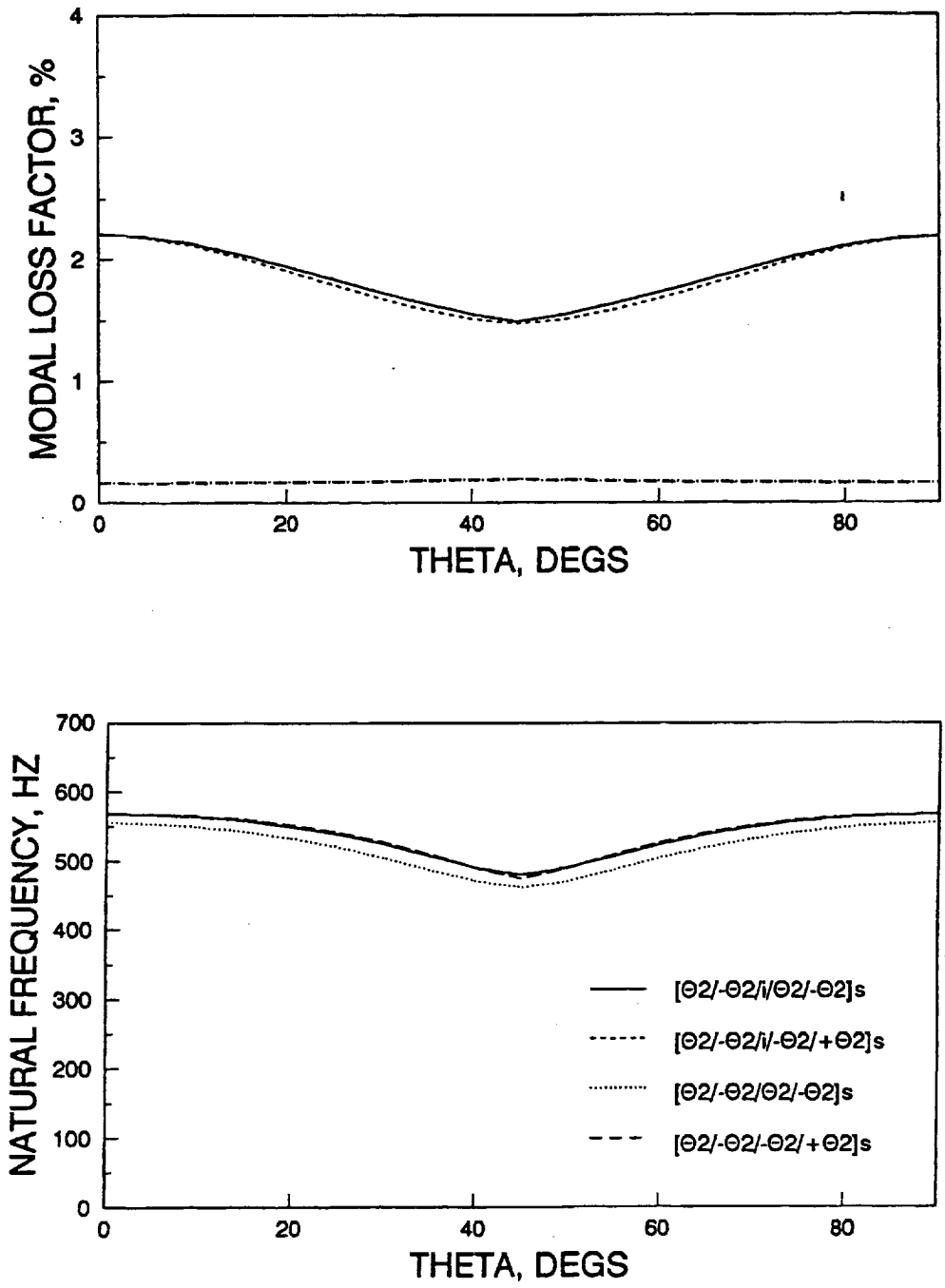

Fig. 6.7 Modal loss factor and natural frequency of angle-ply T300/934 simply supported plates; mode 4.

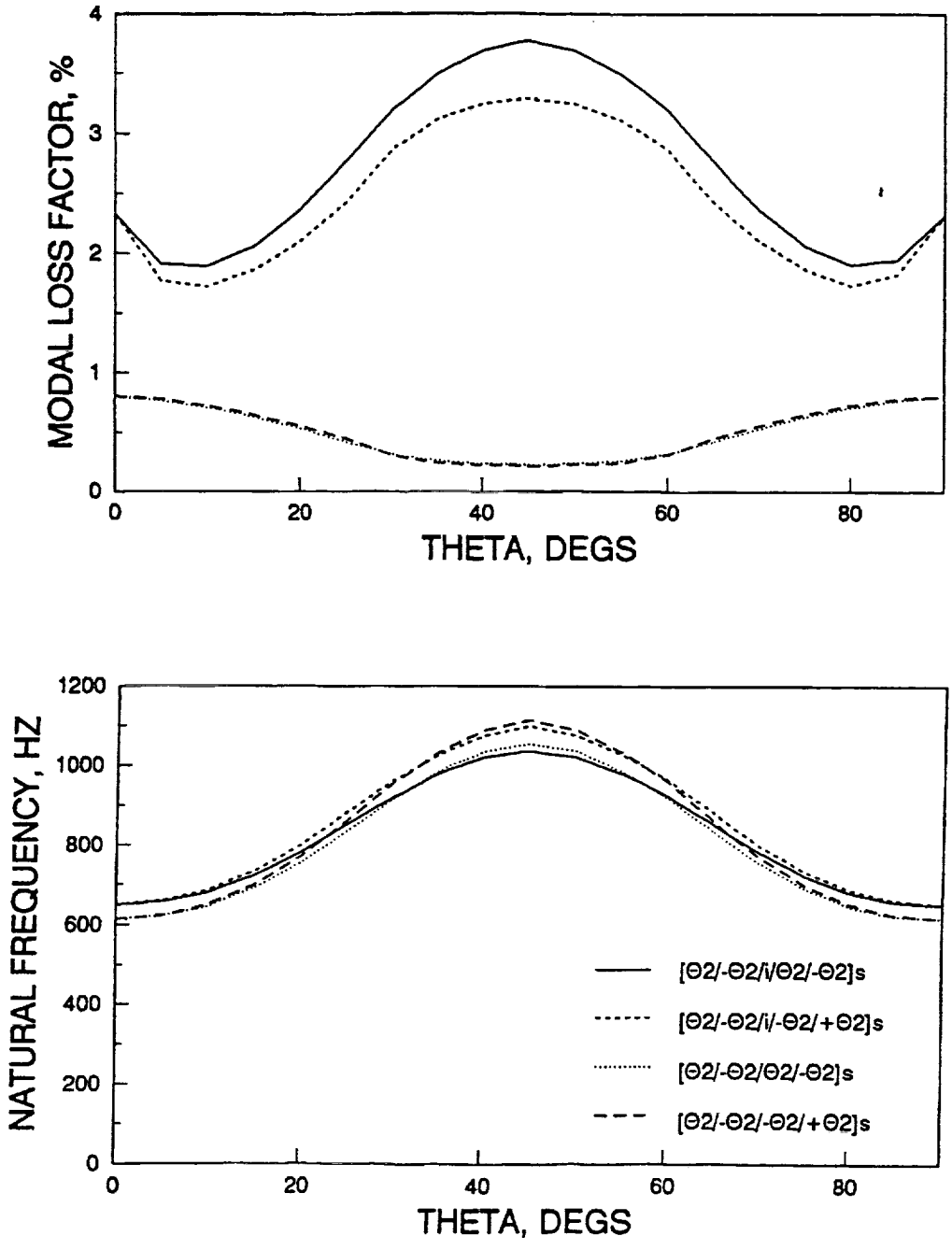

Fig. 6.8 Modal loss factor and natural frequency of angle-ply T300/934 simply supported plates; mode 5.

7. OPTIMAL DESIGN OF THICK COMPOSITE PLATES

7.1 Assumptions

This section presents preliminary evaluation of the developed optimal design methodology for composite plates. For this purpose, the optimal design of a thick composite plate was investigated as a minimal weight problem. Although the design of composite structures for optimal dynamic performance is really a multi-objective task, the present initial investigation maintains simplicity in the objective function. Increases in composite damping may typically result in stiffness/strength reductions and/or mass addition, for this reason, the minimization of weight subject to deflection, natural frequency and modal damping constrains is a reasonable first formulation.

A constrained single-objective problem is described in the following mathematical form:

$$\min \{F_1(d)\} \tag{25}$$

subject to lower and upper bounds on the design vector d and inequality constraints $G(d)$:

$$\{d^L\} \leq \{d\} \leq \{d^U\} \tag{26}$$

$$\{G(d)\} \leq 0 \tag{27}$$

In the rest of the paper, upper and lower values are represented by superscripts L and U respectively.

The objective function in eq. (9) is assumed to be the specific weight per unit area of the plate. The design vector may include fiber volume ratios (FVRs), ply angles, and thicknesses of various sublaminates. Performance constraints include upper bounds on static deflections u^s,

$$\{u^s\} \leq \{u^{sU}\} \tag{28}$$

lower and/or upper bounds on natural frequencies $\{f_{mn}\}$,

$$\{f^L\} \leq \{f_{mn}\} \leq \{f^U\} \tag{29}$$

where, m, n indicate mode order. Additional lower bounds are imposed on each modal damping of the composite plate to ensure that the passive damping of specific modes remains or is "pushed" above desirable limits.

$$\{\eta_{mn}\} \geq \{\eta^L\} \tag{30}$$

Constrains on static and dynamic stresses of composite plies are not included in the present study, but their inclusion is planned as future work.
The constrained optimization mentioned above are solved with the modified feasible directions non-linear programming method[18].

7.2 Optimal Design of a $[0/90]_s$ Plate

Evaluations of the method on Gr/Epoxy cross-ply [0/90]s composite plates were performed. The fiber volume ratio (FVR) and the thickness of the 0 and 90 degs sublaminates were optimized. The initial FVRs were assumed equal to 0.50. The initial thickness of each sublaminate was assumed equal to 0.040 in, that is, the initial thickness of the plate was h=0.16 in. The plates where assumed square ($R=\alpha/\beta=1$), but various length values (α) were considered, in order to investigate the effect of thickness-aspect ratio (α/h) on the resultant optimal designs. An out-of-plane concentrated load of 100 lbs at the center of the plate was applied in all cases.

Apparently, as various values of the plate span α are considered, the natural frequencies and the static deflections will also change, hence, non-dimensional expressions for these expressions were utilized. In the context of CLPT solution[19], for constant R, the non-dimensional expressions of transverse displacement, and natural frequencies may be defined as:

$$\bar{w}(x,y) = \frac{w(x,y)}{4a^2/\pi^4}, \qquad \bar{f}_{mn} = \frac{f_{mn}}{\pi^2/a^2} \tag{31}$$

These expressions were utilized to scale the bounds on constraints (12) and (13) when different values of α were considered, such that geometric similarity in the context of CLPT was maintained. The objective function and modal damping were already non-dimensional. As an example, for a plate of $\alpha=\beta=10$ in, an upper bound on the static defection at the center of the plate was set equal to 0.050 in; lower bounds of 300, 500,

1000, 1000, and 1000 Hz were imposed on the first five natural frequencies of modes (1,1), (1,2), (1,3) and (2,2); and lower bounds of 0.24% was imposed on the corresponding loss factors of the previous five modes. For other values of span length, the constrains were scaled as previously described.

Figs. 7.1-7.5 illustrate the effect of thickness aspect ratio on the resultant objective function and corresponding optimal design parameters. The corresponding α/h was calculated at the initial designs. Because of the scaled objective and constrains, the optimal designs based on CLPT appear independent to the thickness aspect ratio. Clearly, the resultant optimal designs based on DLPT are far more sensitive to aspect ratio than the actual vibrational characteristics (Fig. 4.1). Only at very high aspect ratios ($\alpha/h \approx 200$) comparable optimal designs were attained.

The results illustrate, that at least for the current application, the optimal design of composite plates is very sensitive to the composite mechanics used. Design methods based on classical composite mechanics may produce significant errors even in case of intermediate to low thicknesses. Moreover, the results demonstrate the quality and superiority of the present design method which is based on a more accurate laminate theory. Additional evaluations are planed to be performed in the near future.

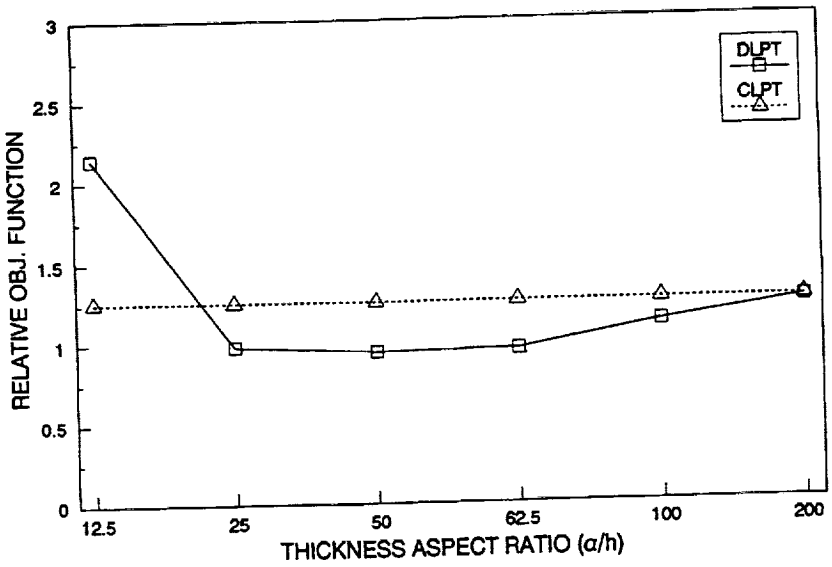

Fig. 7.1 Relative improvements in objective function for various initial thickness aspect ratios (α/h).

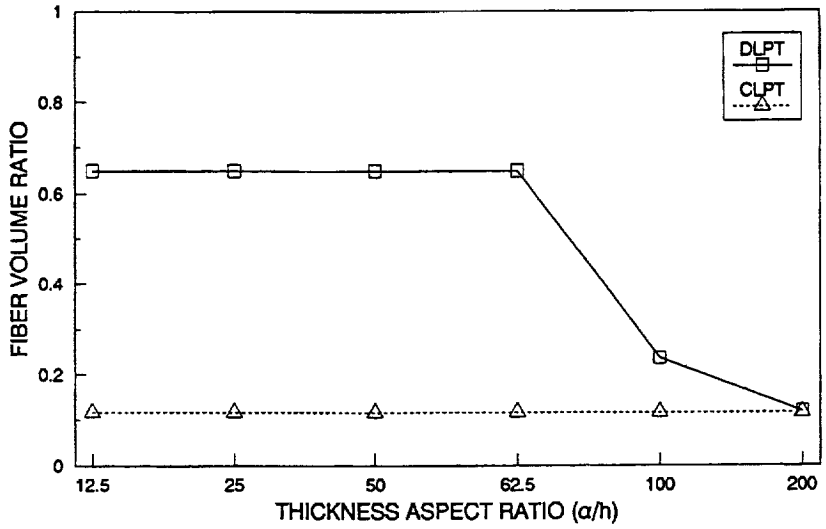

Fig. 7.2 Optimal FVR in 0° sublaminate for various initial thickness aspect ratios (α/h).

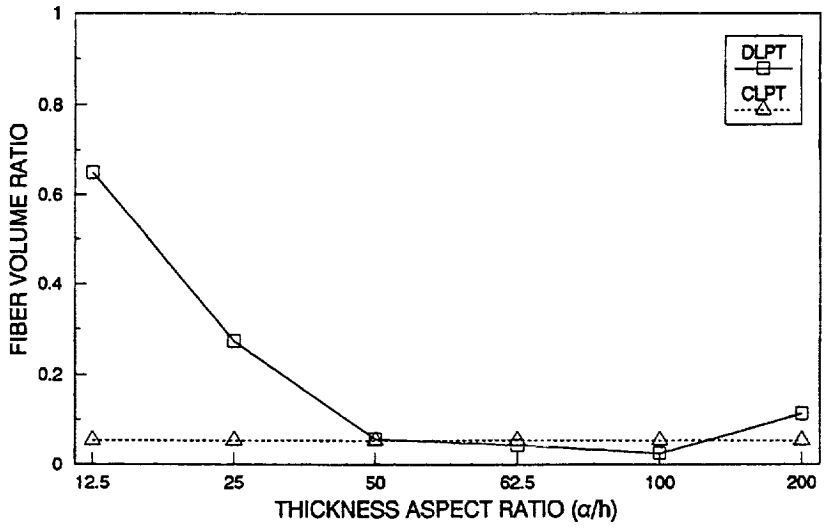

Fig. 7.3 Optimal FVR in 90° sublaminate for various initial thickness aspect ratios (α/h).

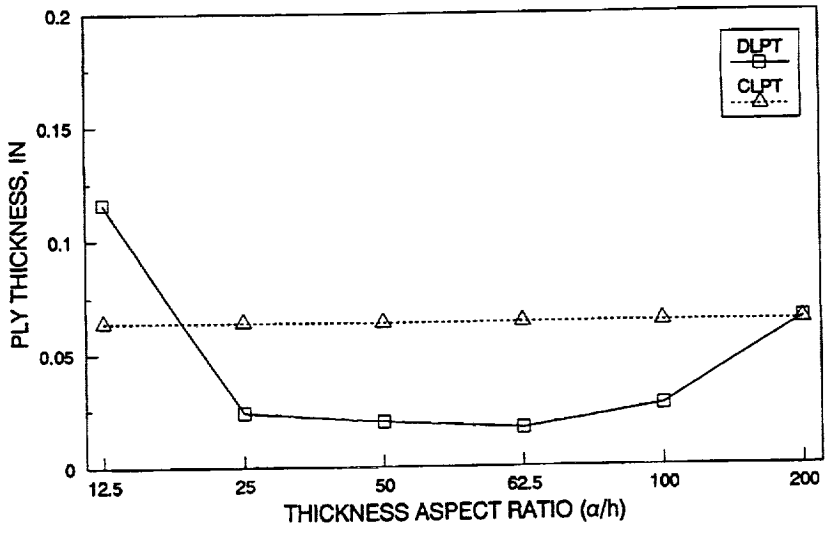

Fig. 7.4 Optimal thickness of 0° sublaminate for various initial thickness aspect ratios (α/h).

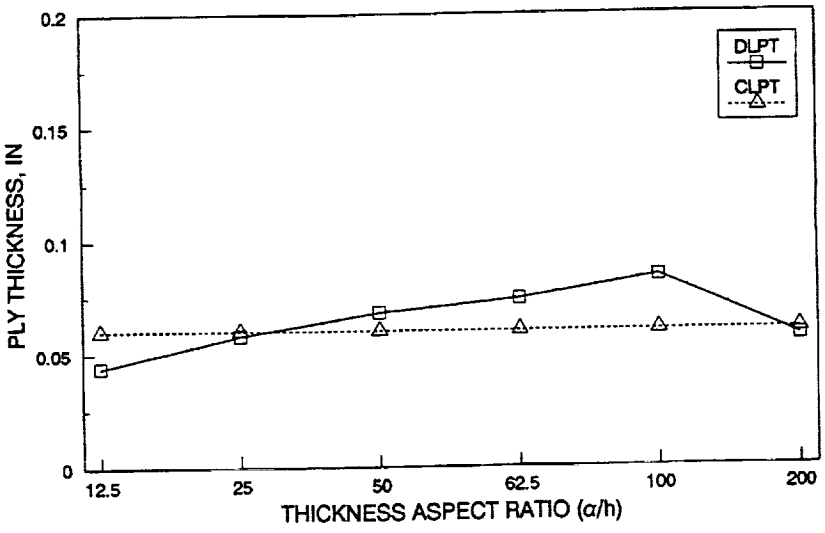

Fig. 7.5 Optimal thickness of 90° sublaminate for various initial thickness aspect ratios (α/h).

CONCLUSIONS AND FUTURE WORK

The development of novel unified damping mechanics for the accurate analysis and design of composites structures was summarized. The work emphasized the need of damping mechanics applicable to represent not only thin, but also thick composite structures, and specialty composite structures with embedded compliant interlaminar layers. The effects of elevated temperature in the dynamic response of the composite structure were also included. The more significant results, accomplishments and prototype software developed as part of this effort were enumerated.

Numerous applications and evaluations of the mechanics illustrated their merit and unique advantages in the case of higher thicknesses, elevated temperatures and interlaminar inhomogeneities. The importance of the mechanics in the optimal design of composite structures was also demonstrated.

Future work is planned in the following areas:

(1) development of a three-dimensional damping theory is planned by incorporating a variable through-the-thickness displacement fields. This theory will establish the upper bound of accuracy, and also will entail the capacity to model the interlaminar normal stress, local impact phenomena, and through-the-thickness wave propagation (vis. noise transmission and acoustic characterization);

(2) the inherent capacity of the theory to represent interlaminar damage in the material will be explored and the effects of delamination on the damping and the dynamic characteristics will be quantified.

(3) extension of the mechanics to model health monitoring conditions in "smart" composite structures with embedded sensors in the form of layers and/or fibers.

REFERENCES

1. Hashin, Z., "Complex Moduli of Viscoelastic Composites - II. Fiber Reinforced Composite Materials," *Int. J. of Solids and Structures,* Vol. 6, 1970, pp. 797-807.

2. Schultz, A. B., and Tsai, S. W., "Measurements of Complex Dynamic Moduli for Laminated Fiber-Reinforced Composites," *J. of Composite Materials,* Vol. 3, 1969, pp. 434-443.

3. Adams, R. D., Fox, M. A. O., Flood, R. J. L., Friend R. J., and Hewitt R. L., "The Dynamic Properties of Unidirectional Carbon and Glass Fiber-Reinforced Plastics in Torsion and Flexure," *J. of Composite Materials,* Vol. 3, 1969, pp. 594-603.

4. Siu, C. C., and Bert, C. W., "Sinusoidal Response of Composite-Material Plates with Material Damping," *ASME J. of Engineering for Industry,* May 1974, pp. 603-610.

5. Sun, C. T., Chaturvedi, S. K., and Gibson, R. F., "Internal Damping of Short-Fiber Reinforced Polymer Matrix Composites," *Computers and Structures,* Vol. 20, No. 1-3, 1985, pp. 391-400.

6. Suarez, S. A., Gibson, R. F., Sun, C. T., and Chaturvedi, S. K., "The Influence of Fiber Length and Fiber Orientation on Damping and Stiffness of Polymer Composite Materials," *Experimental Mechanics,* Vol. 26, No. 2, 1986, pp. 175-184.

7. Saravanos, D. A. and Chamis, C. C. "Unified Micromechanics of Damping for Unidirectional and Off-Axis Fiber Composites," *J. of Composites Technology and Research,* Vol. 12, No. 1, 1990, pp. 31-40.

8. Saravanos, D. A. and Chamis, C. C. "Mechanics of Damping for Fiber Composite Laminates Including Hygro-Thermal Effects," *AIAA J.,* Vol. 28, No. 10, 1990, pp. 1813-1819.

9. Ni, R. G., and Adams, R. D., " The Damping and Dynamic Moduli of Symmetric Laminated Composite Beams -- Theoretical and Experimental Results," *J. of Composite Materials,* Vol. 18, 1984, pp. 104-121.

10. Bicos, A. S. and Springer, G. S. "Vibrational Characteristics of Composite Panels with Cutouts," *AIAA Journal,* Vol. 27, Aug. 1989, pp. 1116-1122.

11. Saravanos, D. A. and Chamis, C. C. "Computational Simulation of Damping in Composite Structures," *J. of Reinforced Plastics and Composites,* Vol. 10, 1991, pp. 256-278.

12. Alam, N. and Asnani, N. T. "Vibration and Damping Analysis of Fibre Reinforced Composite Material Plates," *J. of Composite Materials,* Vol. 20, 1986, pp. 2-18.

13. Saravanos, D. A. and Pereira J. M. "The Effects of Interlaminar Damping Layers on the Dynamic Response of Composite Structures," *AIAA J.,* in press; (also, NASA TM 104497).

14. Noor, A. K. and Burton, S. W., "Assessment of Computational Models for Multilayer Composite Shells," *Applied Mechanics Reviews,* Vol. 43, No. 4, 1990, pp. 67-96.

15. Barbero, E. J., Reddy, J. N. and Teply, J., "An Accurate Determination of Stresses in Thick Composite Laminates Using a Generalized Plate Theory," *Int. J. for Numerical Methods in Engineering,* Vol. 29, 1990, pp. 1-14.

16. Drake M. L., "Damping Properties of Various Materials," Research Lab., Dayton University, Dayton, OH, *Report AFWAL-TR-88-4248*, March 1989.

17 Pereira M. J., "Dynamic Response of Composite Plates with Interlaminar Damping Layers," *Proceedings, Symposium on Vibroacoustic Characterization of Materials and Structures*, ASME Winter Annual Meeting, Anaheim, California, Nov. 8-13, 1992

18. Vanderplaats, G. N., "A Robust Feasible Directions Algorithm for Design Synthesis," *Proceedings, 24th AIAA/ASME/ASCE/AHS Structures, Structural Dynamics, and Materials Conference,* Lake Tahoe, NV, 1983.

19. Whitney J. M., "Specially Orthotropic Plates," *Structural Analysis of Laminated Anisotropic Plates*, Technomic Publishing Co., Lancaster, PA, 1987, pp. 87-123.

APPENDIX I: Nomenclature

$[A]$, $[B^j]$, $[D^{jm}]$	Extensional, coupling and flexural/shear laminate stiffness matrices.
$[A_d]$, $[B_d{}^j]$, $[D_d{}^{jm}]$	Extensional, coupling and flexural/shear laminate damping matrices.
$[A_m]$, $[B_m{}^j]$, $[D_m{}^{jm}]$	Extensional, coupling and flexural/shear laminate mass matrices.
$[C]$	Damping matrix, structural
E	Normal modulus
$F^j(z)$	Interpolation function
G	Shear modulus
h	cross-section thickness
$[K]$	Stiffness matrix, structural
l	beam length
$[M]$	Mass matrix, structural
N^o, N^j	Midplane and generalized stress resultants
$[Q]$	Composite stiffness matrix
$[R]$	Strain shape function
S	Maximum stored strain energy, per cycle
u, v, w	Axial, transverse and through-the-thickness displacements respectively
x, y, z	Axial, transverse and through-the-thickness structural axes.
α, β	Plate dimensions along x and y axes, respectively
ΔS	Dissipated strain energy, per cycle
$\{\epsilon\}$	Engineering strain tensor
η	Loss factor
ν	Poisson's ratio
ρ	Mass density
ϕ	Shape function
ω	Natural frequency
ψ	Specific damping capacity

Subscripts

c	Composite (structural coordinates)
e	Element
l	Composite (material coordinates)
L	Laminate
m	Mode order, x direction
n	Mode order, y direction
1	Normal longitudinal (direction 11)
2	Normal transverse, in plane (direction 22)
3	Normal transverse, out of plane (direction 33)

4	Interlaminar shear (direction 23)
5	Interlaminar shear (direction 13)
6	In-plane shear (direction 12)

Superscripts

o	Midplane
j	Generalized

APPENDIX II: Fundamental Composite Mechanics

Off-axis ply stiffness matrix $[Q_c]$:

$$\{\sigma_c\} = [Q_c]\{e_c\}$$

$$[Q_c] = [R]^{-1}[Q_l][R]^{-T}$$

where $[Q_l]$ is the stiffness matrix in the material axes. The transformation matrices are:

$$[R] = \begin{bmatrix} m^2 & n^2 & 0 & 0 & 0 & 2mn \\ n^2 & m^2 & 0 & 0 & 0 & -2mn \\ 0 & 0 & 1 & 0 & 0 & 0 \\ 0 & 0 & 0 & m & -n & 0 \\ 0 & 0 & 0 & n & m & 0 \\ -mn & mn & 0 & 0 & 0 & m^2-n^2 \end{bmatrix}, \qquad m = \cos\theta, \quad n = \sin\theta$$

$$[R]^{-1} = [R(-\theta)]$$

On-axis damping matrix:

$$[\eta_l] = diag\ [\ \eta_{l11}, \eta_{l22}, \eta_{l33}, \eta_{l44}, \eta_{l55}, \eta_{l66}\ ]$$

The off-axis ply damping matrix is:

$$[\eta_c] = [R]^T[\eta_l][R]^{-T}$$

$$[\eta_c] = \begin{bmatrix} \eta_{c11} & \eta_{c12} & 0 & 0 & 0 & \eta_{c16} \\ \eta_{c21} & \eta_{c22} & 0 & 0 & 0 & \eta_{c26} \\ 0 & 0 & \eta_{c33} & 0 & 0 & 0 \\ 0 & 0 & 0 & \eta_{c44} & \eta_{c45} & 0 \\ 0 & 0 & 0 & \eta_{c54} & \eta_{c55} & 0 \\ \eta_{c61} & \eta_{c62} & 0 & 0 & 0 & \eta_{c66} \end{bmatrix}$$

REPORT DOCUMENTATION PAGE

Form Approved
OMB No. 0704-0188

1. AGENCY USE ONLY (*Leave blank*)	2. REPORT DATE	3. REPORT TYPE AND DATES COVERED
	March 1993	Final Contractor Report

4. TITLE AND SUBTITLE

Integrated Analysis and Design of Thick Composite Structures for Optimal Passive Damping Characteristics

5. FUNDING NUMBERS

WU-505-63-5B
NCC3-208/4

6. AUTHOR(S)

D.A. Saravanos

7. PERFORMING ORGANIZATION NAME(S) AND ADDRESS(ES)

Ohio Aerospace Institute
22800 Cedar Point Road
Brook Park, Ohio 44142

8. PERFORMING ORGANIZATION REPORT NUMBER

E-7676

9. SPONSORING/MONITORING AGENCY NAMES(S) AND ADDRESS(ES)

National Aeronautics and Space Administration
Lewis Research Center
Cleveland, Ohio 44135-3191

10. SPONSORING/MONITORING AGENCY REPORT NUMBER

NASA CR-190783

11. SUPPLEMENTARY NOTES

Project Manager, Christos C. Chamis, Structures Division, (216) 433-3252.

12a. DISTRIBUTION/AVAILABILITY STATEMENT

Unclassified - Unlimited
Subject Category 24

12b. DISTRIBUTION CODE

13. ABSTRACT ***(Maximum 200 words)***

The development of novel composite mechanics for the analysis of damping in composite laminates and structures, and the more significant results of this effort are summarized. Laminate mechanics based on piecewise continuous in-plane displacement fields are described that can represent both intralaminar stresses and interlaminar shear stresses and the associated effects on the stiffness and damping characteristics of a composite laminate. Among other features, the mechanics can accurately model the static and damped dynamic response of either thin or thick composite laminates, as well as, specialty laminates with embedded compliant damping layers. The discrete laminate damping theory is further incorporated into structural analysis methods. In this context, an exact semi-analytical method for the simulation of the damped dynamic response of composite plates was developed. A finite element based method and a specialty four-node plate element was also developed for the analysis of composite structures of variable shape and boundary conditions. Numerous evaluations and applications demonstrate the quality and superiority of the mechanics in predicting the damped dynamic characteristics of composite structures. Finally, additional development was focused towards the development of optimal tailoring methods for the design of thick composite structures based on the developed analytical capability. Applications on composite plates illustrated the influence of composite mechanics in the optimal design of composites and the potential for significant deviations in the resultant designs when more simplified (classical) laminate theories are used.

14. SUBJECT TERMS

Composites; Damping; Thick composites; Damping layers; Engineered materials; Compliant layers; Laminates; Structures; Dynamic analysis; Natural frequencies; Interlaminar effects; Finite elements; Optimal design

15. NUMBER OF PAGES

62

16. PRICE CODE

A04

17. SECURITY CLASSIFICATION OF REPORT	18. SECURITY CLASSIFICATION OF THIS PAGE	19. SECURITY CLASSIFICATION OF ABSTRACT	20. LIMITATION OF ABSTRACT
Unclassified	Unclassified	Unclassified	